



## **Abstract**

The development of metal stable isotopes as tools in paleoceanography requires a thorough understanding of their modern marine cycling. To date, no Cu isotope data has been published for modern sediments deposited under low oxygen conditions. We present data encompassing a broad spectrum of hydrographic and redox regimes, including continental margin and euxinic (sulphide-containing) settings. Taken together with previously published data from oxic settings, these data indicate that the modern oceanic sink for Cu has a surprisingly homogeneous isotopic composition of about +0.3‰ ( $\delta^{65}\text{Cu}$ , relative to NIST SRM 976). We suggest that this signature reflects one of two specific water-column processes: (1) an equilibrium isotope fractionation between soluble, isotopically heavy, Cu complexed to strong organic ligands and an isotopically light pool sorbed to particles that deliver Cu to the sediment, or (2) an equilibrium isotope fractionation between the same isotopically heavy ligand-bound pool and the particle reactive free  $\text{Cu}^{2+}$  species, with the latter being scavenged by particulates and thereby delivered to the sediment. An output flux of about +0.3‰ into sediments is isotopically light relative to the known inputs to the ocean (at around +0.6‰) and the seawater value of +0.6 to +0.9‰, suggesting the presence of an as yet unidentified isotopically light source of Cu to the oceans. We hypothesize that this source may be hydrothermal, or may result from the partial dissolution of continentally derived particles.

## 1 **1. Introduction**

2  
3 Copper (Cu) is biologically essential, but the free  $\text{Cu}^{2+}$  form is also toxic, even at  
4 extremely low concentrations (e.g., Moffett and Brand, 1996). Aqueous Cu speciation is,  
5 however, almost universally dictated by complexation to strong organic ligands (e.g.,  
6 Elderfield, 1981; Coale and Bruland, 1988; Gordon et al., 1996; Skrabal et al., 1997; 2000;  
7 Wells et al., 1998; Muller et al., 2001; Laglera and van den Berg, 2003; Shank et al.,  
8 2004a; 2004b; Bruland and Lohan, 2003; Moffett and Dupont, 2007). In addition to its  
9 biological function, Cu is particle reactive, and its speciation and solubility are sensitive to  
10 changes in redox conditions. Understanding the balance of these competing processes in  
11 controlling the oceanic distribution of Cu and its isotopes has been the subject of a large  
12 number of studies (e.g., Boyle et al., 1977; Bruland, 1980; Saager et al., 1992; Bermin et  
13 al., 2006; Vance et al., 2008; Thompson et al., 2014; Takano et al., 2014; Little et al.,  
14 2014a,b).

15  
16 Isotopes provide insight into the mechanisms of metal cycling, with specific isotope  
17 signatures attributable to particular processes (e.g., Welch et al., 2003; Barling and Anbar,  
18 2004; Severmann et al., 2008; Wasylenki et al., 2011; Peacock and Moon, 2012; Xue et al.,  
19 2013; Little et al., 2014b; Vance et al., 2016a). Isotopic measurements are also a useful  
20 way to place constraints on oceanic mass balance (e.g., Zhu and Macdougall, 1998;  
21 Schmitt et al., 2003; Tipper et al., 2006; 2010; Nielsen et al., 2006; Archer and Vance,  
22 2008; Conway and John, 2014; Little et al., 2014a). Based on an analysis of the known  
23 inputs and outputs of Cu and its isotopes to the modern ocean, Little et al. (2014a)  
24 highlighted an imbalance in the oceanic budget of Cu. Assuming that the cycle is in steady  
25 state, these authors suggested the presence of an as yet unidentified isotopically heavy Cu  
26 sink (Little et al., 2014a).

27  
28 No Cu isotope data exist to date for reducing sedimentary settings, making them a prime  
29 candidate for the missing Cu sink. Reducing depositional environments include locations  
30 where the water column is euxinic (sulphide-containing), such as the Black Sea and  
31 Cariaco Basin, and those in which dissolved oxygen concentrations are negligible but  
32 sulphide is either absent or restricted to pore-waters. The latter are typical of oxygen  
33 minimum zones (OMZs) along productive continental margins. Copper is insoluble under

34 reducing conditions. Consequently, water column removal of Cu is nearly quantitative  
35 below the redoxcline of the euxinic Black Sea and Cariaco Basin (Jacobs et al., 1987;  
36 Haraldsson and Westerlund, 1988; Tankéré et al., 2001), and variable Cu enrichments have  
37 previously been observed in reducing sediments (e.g., Francois, 1988; Calvert and  
38 Perderson, 1993; Algeo and Maynard, 2004; Brumsack, 2006; Little et al., 2015). An iron-  
39 rich (ferruginous) pore water profile from the oxygen-poor Santa Monica basin  
40 (California) shows evidence of Cu diffusion into sediments and no detectable Cu in pore  
41 waters within a few centimetres of the sediment-water interface, suggesting diagenetic  
42 removal of Cu into sedimentary sulphide phases (Shaw et al., 1990). Generally, however,  
43 there is a lack of similar pore water studies from sediment underlying anoxic ocean waters.  
44

45 Reduction of Cu(II) to Cu(I) is likely to be associated with a light isotope fractionation into  
46 the reduced phase (e.g., Zhu et al., 2002; Ehrlich et al., 2004; Fujii et al., 2013, Sherman,  
47 2013), i.e., fractionation in the opposite direction to that required for an isotopically heavy  
48 Cu sink. However, quantitative removal from the water column implies that the authigenic  
49 Cu isotope values of sediments deposited under euxinic conditions should reflect the Cu  
50 isotope composition of the dissolved pool of the oceans, as observed previously for similar  
51 metal isotope systems (e.g., Mo, Zn, Cr; Barling et al., 2001; Nägler et al., 2011; Reinhard  
52 et al., 2014; Vance et al., 2016a). The dissolved Cu pool in seawater is, indeed, isotopically  
53 heavy, at +0.6 to +0.9‰ (Vance et al., 2008; Thompson et al., 2014; Takano et al., 2014).  
54

55 Euxinic sites play a relatively minor role as a global sink for trace metals in the modern  
56 ocean, however, due to the restricted areal extent of such conditions (e.g., Emerson and  
57 Huested, 1991; Morford and Emerson, 1999; Poulson Brucker et al., 2009; Little et al.,  
58 2015). Today, upwelling margins with prominent OMZs are likely a much more important  
59 sink for trace metals (e.g., Morford and Emerson, 1999; Böning et al., 2004; 2009;  
60 McManus et al., 2006; Poulson Brucker et al., 2009; Little et al., 2015; 2016), and  
61 forecasts suggest their expansion in a warming world (Stramma et al., 2008; Keeling et al.,  
62 2010). To date, only one estimate has been made of the role of upwelling margin sediments  
63 in the oceanic mass balance of Cu (Little et al., 2015), and the isotope composition of the  
64 flux of Cu into margin sediments is unknown. In this study, we present Cu isotope data for  
65 a wide range of reducing environments, including the euxinic Black Sea and Cariaco  
66 Basin, and multiple continental margin sites. This dataset provides considerably improved  
67 constraints on the reducing sedimentary sink for Cu.

68

## 69 **2. Study sites**

70

### 71 *2.1 The Black Sea*

72 Open ocean euxinia is thought to have been more prevalent at times during Earth's history,  
73 particularly along productive margins (Canfield, 1998; Li et al., 2010a; Lyons et al., 2014).

74 Today, however, euxinia is largely restricted to marginal basins, with the Black Sea as the  
75 world's largest permanently euxinic basin. The Black Sea is thus frequently cited as an

76 analogue of the Precambrian oceans and for periods of widespread anoxia during the

77 Phanerozoic. Euxinia below ~100 m water depth in the Black Sea is the result of a positive

78 water balance, moderate primary production, and restricted circulation, with limited inflow

79 and outflow to the Mediterranean Sea via the narrow (0.76 – 3.6 km wide) and shallow

80 (<110 m deep) Bosphorus Strait. Total sulphide concentrations increase to 380  $\mu\text{M}$  at 2200

81 m water depth and are associated with near quantitative removal of Cu from the dissolved

82 phase (Haraldsson and Westerlund, 1991; Tankéré et al., 2001). The samples analysed in

83 this study have been described previously (Lyons, 1991; Little et al., 2015). Two deep sites

84 underlie the euxinic water column (stations 9 and 14; Fig. 1), while two others are from the

85 shallow shelf and underlie oxic water (stations 16 and 16B; Fig. 1). Station 16B was

86 recovered from a depth close to the modern day chemocline. A broad array of

87 sedimentological observations (Lyons, 1991) and complementary geochemical analyses

88 has been made on these sediments. These include C-S-Fe systematics (Lyons and Berner,

89 1992; Lyons et al., 1993), S-isotope trends (Lyons, 1997), Fe speciation and isotope

90 patterns (Lyons and Severmann, 2006; Severmann et al., 2008), Mo abundance and isotope

91 compositions (Arnold et al., 2004; Algeo and Lyons, 2006), trace metal concentrations

92 (Little et al., 2015) and Zn and Ni isotope analyses (Vance et al., 2016a). We present bulk

93 sediment Cu isotope data for a total of 31 samples from the four locations, all of which are

94 confined to the upper ~25 cm of the sediment pile at each locality (Fig. 1; see also Little et  
95 al., 2015).

96

### 97 *2.2 The Cariaco Basin*

98 The Cariaco Basin is the world's second largest anoxic basin (Fig. 1, Table 1). It is located

99 on the northern continental shelf off Venezuela and contrasts with the Black Sea in that it

100 has a less restricted hydrographic setting, higher productivity, and higher sedimentation

101 rate. The Cariaco Basin has been euxinic since the last deglaciation (Haug et al., 1998;

102 Dean et al., 1999; Peterson et al., 2000), but euxinia in the water column is less extreme  
103 than that in the Black Sea, with peak total sulphide concentrations of ~65  $\mu\text{M}$  (Li et al.,  
104 2010b; 2011). Again, Cu removal from the water column is observed due to the presence  
105 of sulphide (Jacobs et al., 1987). The 22 drill core samples (20 cm to 8 m depth) included  
106 in this study from ODP Site 1002 span the oxic-euxinic transition at 14.5 ka and the  
107 associated redox-related geochemical changes in the core have previously been studied in  
108 detail (Lyons et al., 2003; Werne et al., 2003; Lyons and Severmann, 2006; Reinhard et al.,  
109 2014; Little et al., 2015).

110

### 111 *2.3 Continental Margin sites*

#### 112 *2.3.1 California Borderland basins*

113 The Southern California Bight is a region of elevated primary production, primarily due to  
114 coastal upwelling (e.g., Eppley, 1992; Macías et al., 2012). The resultant carbon flux to  
115 depth, in combination with related ocean circulation patterns, generates oxygen-deficient  
116 waters at depths of 200 m to 1000 m along the margin. The Southern California Borderland  
117 basins exhibit even lower oxygen contents than equivalent depths along the open margin  
118 because the silled topography restricts mixing of basin waters with surrounding seawater  
119 (e.g. Emery, 1954; Berelson, 1991). The samples used in this study come from four of the  
120 Borderland basins: Santa Barbara, Santa Monica, San Nicolas, and Tanner Basin (Fig. 1).  
121 These settings have been characterised geochemically, and samples for this study were  
122 taken from expeditions described previously (e.g., McManus et al., 1997; McManus et al.,  
123 1998; McManus et al., 2006; Poulson-Brucker et al., 2009; Little et al., 2016).

124

125 The Santa Barbara and Santa Monica basins are near shore and have sill depths within the  
126 region's OMZ. The Santa Barbara basin is the most reducing of the four Borderland basins  
127 included for study, though the core studied was sampled just below the sill (sill: 475 m,  
128 core site: 493 m; Poulson-Brucker et al., 2009). Dissolved sulphide is present to varying  
129 degrees within the shallow sediment package and has been observed at low (<15 nM)  
130 levels in the water column (e.g., Kuwabara et al., 1999; Zheng et al., 2000). These  
131 observations, coupled with the fact that the shallow pore fluids (upper 3–8 cm, with  
132 sulphide appearing below) are ferruginous (e.g., Kuwabara et al., 1999; Zheng et al.,  
133 2000), imply that iron reduction and sulphate reduction are dominant electron transfer  
134 pathways within the shallow sediment package. The mass accumulation rate in Santa

135 Barbara is the highest of all the sites studied (Table 1), which is largely the result of high  
136 fluxes of lithogenic material (Thunell et al., 1995).

137

138 The Santa Monica sill is at 740 m, the basin floor is at 910 m, and the sediment core was  
139 collected at 905 m. Bottom-water oxygen concentrations vary within the basin but are  
140 generally 2 - 10  $\mu\text{M}$  (Berelson, 1991; Stott et al., 2000; Berelson et al., 2005; McManus et  
141 al., 2006). Like Santa Barbara basin, shallow pore fluids in Santa Monica are ferruginous  
142 (e.g., Shaw et al., 1990; McManus et al., 1997; 1998). Although Shaw et al. (1990) report a  
143 thin ( $\sim 1$  cm) layer of extractable Fe at the sediment-water boundary, transfer of dissolved  
144 Fe occurs across this boundary (McManus et al., 1997; Elrod et al., 1991; Severmann et al.,  
145 2010). To our knowledge there are no reports of shallow sediment-column or bottom-water  
146 accumulation of dissolved sulphide; net sulphate reduction is nevertheless an important  
147 pathway for electron transport, as manifest in iron sulphide minerals that form within the  
148 sediments (Berelson et al., 1996).

149

150 The offshore basins, San Nicolas and Tanner, have sill depths at 1100 m and 1160 m,  
151 respectively, below the depth of the most intense oxygen deficiency. Tanner Basin is  
152 further offshore than San Nicolas (Emery, 1960). Maximum water depths in the San  
153 Nicolas basin are 1832 m (core collected at 1750 m), with bottom-water oxygen contents  
154 of  $\sim 30$   $\mu\text{M}$  (Shaw et al., 1990). Pore fluids from the upper 10 cm are rich in dissolved Mn,  
155 with strong increases in Mn appearing just below the sediment-water interface (Shaw et al.,  
156 1990). Dissolved Fe concentrations increase below  $\sim 2$  cm, with much lower Fe  
157 concentrations in the upper sediment package compared to those in the basins nearer to  
158 shore (Shaw et al., 1990). The Tanner Basin reaches a maximum depth of 1550 m, and the  
159 core was collected at 1514 m. Bottom water oxygen contents are  $\sim 30$   $\mu\text{M}$ . Sediments in  
160 this basin also exhibit pore fluid Fe and Mn enrichments, but the concentrations of both are  
161 lower than those in San Nicolas Basin sediments (c.f., Shaw et al., 1990; McManus et al.,  
162 1997; 1998). Despite differences in dissolved metal concentrations, these two basins are  
163 quite similar diagenetically, with Tanner having an estimated sediment depth of oxygen  
164 penetration that is slightly shallower than in San Nicolas (e.g., 0.4 vs. 0.5 cm, Berelson et  
165 al., 1996) and slightly higher total organic carbon contents ( $\sim 6$  wt% vs.  $\sim 4.5$  wt%; Little et  
166 al., 2016).

167

168

169 *2.3.2 Mexican Margin*

170 Oxygen deficiency is more pronounced along the Mexican margin compared to the  
171 California margin, with oxygen concentrations of  $< 1 \mu\text{M}$  at our study sites (Chong et al.,  
172 2012). This OMZ extends more than 1500 km off the coast of Mexico (Sansone et al.,  
173 2004), and anaerobic diagenetic processes dominate in sediments where the OMZ  
174 intercepts the seafloor (Berelson et al., 2005). Of the three sites included in this study, two  
175 are from the open ocean margin off Baja California (Magdalena and the Soledad Basin),  
176 and the other is from the Pescadero Slope, which is at the eastern edge of the mouth of the  
177 Gulf of California (Chong et al., 2012) (Fig. 1).

178

179 The Magdalena site is situated on the western margin of Baja California at 692 m water  
180 depth. The upper 1 - 2 cm of the sediment core is bioturbated, and organic carbon contents  
181 are particularly high ( $\sim 11\%$ ). Dissolved sulphide appears in pore waters at 3 cm depth ( $2$   
182  $\mu\text{M}$ ) and increases rapidly at depths greater than 20 cm (Chong et al., 2012). The Soledad  
183 Basin is also on the western side of Baja California and has an effective sill depth of  $\sim 250$   
184 m (Silverberg et al., 2004). The core studied here was collected at 544 m water depth, close  
185 to the deepest point of the basin (545 m). Sediments at this site are laminated (including  
186 extensive traceable coccolith laminae; van Geen et al., 2003), with sulphide ( $\sim 10 \mu\text{M}$ ) in  
187 pore waters close to the sediment-water interface and increasing below 8 cm (to  $> 40 \mu\text{M}$ )  
188 (Chong et al., 2012). Because of the high sulphide concentrations, dissolved iron is titrated  
189 from the pore fluids at relatively shallow depths (Chong et al., 2012). Clastic input on the  
190 open ocean side of Baja California is low, but sediment accumulation rates are high,  
191 particularly in the Soledad Basin, due to elevated productivity (Sansone et al., 2004; Table  
192 1). Clastic input is high along the Pescadero slope, due to the location of this coring site on  
193 the eastern edge of the mouth of the Gulf of California, where it receives continental  
194 drainage from the Sierra Madre Occidental Mountains (e.g., Berelson et al., 2005; Chong  
195 et al., 2012). The laminated sediment core discussed in this study was taken at 616 m, close  
196 to the centre of the OMZ (at  $\sim 600$  m). High concentrations of dissolved Fe have been  
197 reported from the pore waters of this site, rising from near zero to  $260 \mu\text{M}$  within the first 2  
198 cm (Chong et al., 2012), compared to peaks of  $\sim 10 \mu\text{M}$  at 3 cm for the Magdalena site and  
199 a  $\sim 65 \mu\text{M}$  peak in the upper 1 cm of the Soledad sediment core. Chong et al. (2012)  
200 classified the Pescadero site as Fe-rich, Magdalena as Fe-rich/sulphidic, and Soledad Basin  
201 as sulphidic.

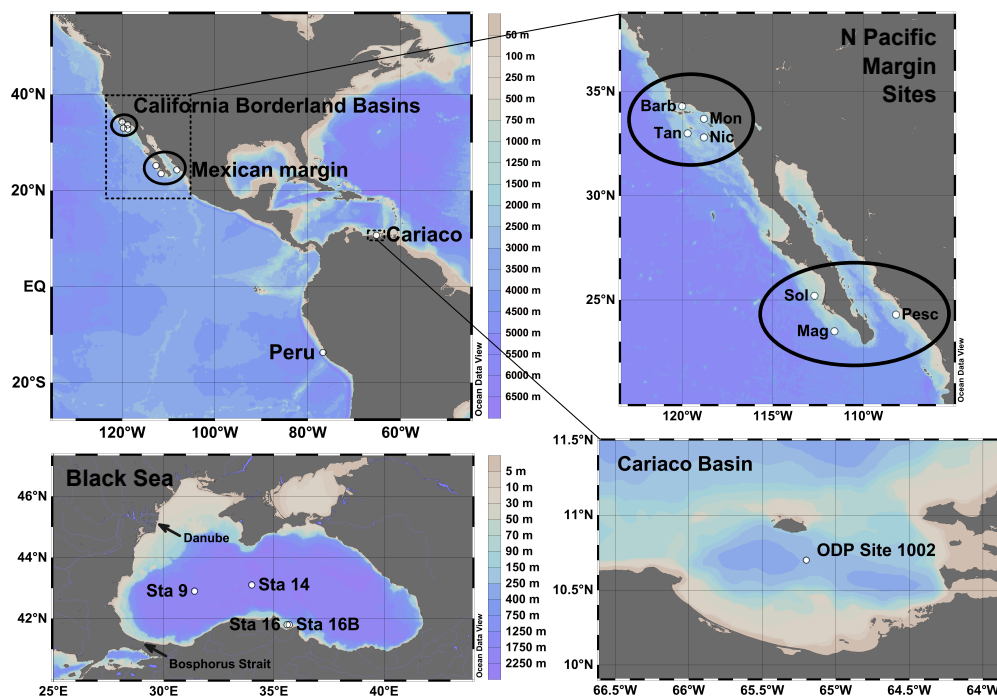
202

203 2.3.3 Peru Margin

204 The Peru margin is an open ocean margin setting with high upwelling-driven productivity  
205 and an associated intense OMZ at depths of ~100 to 700 m (Emeis et al., 1991; Lückge and  
206 Reinhardt. 2000). The core used in our study (Fig. 1, see also McManus et al., 2006; Little  
207 et al., 2015; 2016) was collected at 264 m, with bottom-water oxygen concentrations of  
208 <10  $\mu\text{M}$ . Bulk sediments contain ~15% organic carbon and >1% total sulphur (McManus  
209 et al., 2006; Little et al., 2016). This combination of high organic carbon and low oxygen  
210 results in intense anerobic diagenesis, with prior work demonstrating the potential for  
211 reduced iron fluxes across the sediment water interface (Noffke et al., 2012; Scholz et al.,  
212 2014). Episodic efflux of sulphide has also been reported further south along the Peruvian  
213 margin (Schunck et al., 2013).

214

215 **Figure 1.** Locations of sites included for study. The Peru margin site (site MC82; Table 1;  
216 McManus et al., 2006) is from the core of the Peruvian OMZ. The California Borderland  
217 Basins (N Pacific Margin Sites inset) comprise: Barb – Santa Barbara Basin, Mon – Santa  
218 Monica Basin, Nic – San Nicolas Basin and Tan – Tanner Basin. The Mexican margin  
219 sites (N Pacific Margin Sites inset) comprise: Sol – Soledad Basin, Mag – Magdalena  
220 margin and Pesc – Pescadero Slope. The Cariaco Basin samples are from spliced cores A  
221 and B at Site 1002 of Leg 165 of the Ocean Drilling Program (see inset). Samples from  
222 four Black Sea stations were analysed: two underly the deep euxinic water column  
223 (Stations 9 and 14) and two are from the shallow oxic shelf region (Stations 16 and 16B).  
224 Maps were made using Ocean Data View software (odv.awi.de; Schlitzer, 2015).



225

226

227

### 228 3. Methods

229

#### 230 3.1 Elemental concentrations and Cu isotope data

231 All work was carried out under trace metal clean conditions, with MilliQ water (18.2Ω)  
232 and Savillex PFA labware. Acids and reagents used were either ultrapure (HF, H<sub>2</sub>O<sub>2</sub>) or  
233 double distilled (HNO<sub>3</sub>, HCl). Sample digestion and analytical methods have been  
234 described previously (Little et al., 2014a; 2015). In brief, dilute nitric acid was added  
235 dropwise to 50-500 mg of powdered sediment until effervescence ceased (signalling  
236 complete dissolution of carbonate). The sediment was then digested in a 3:1 mix of  
237 concentrated HF and concentrated HNO<sub>3</sub> for 48 hours. Digestion was followed by triple  
238 treatment with concentrated HNO<sub>3</sub> to remove fluoride salts before dissolution in 7M HCl.  
239 An aliquot of these solutions was analysed for multi-element concentrations on a  
240 ThermoFinnigan Element 2 at the University of Bristol or a ThermoFinnigan Element XR  
241 at ETH Zürich.

242

243 After elemental analysis, an aliquot of the total digest solution was taken for Cu isotope  
244 purification using a two-stage anion exchange procedure (Bio-Rad AG MP-1M resin)  
245 modified from Maréchal et al. (1999) and detailed previously (Archer and Vance, 2004;  
246 Vance et al., 2008; Little et al., 2014a). Final Cu concentrations for analysis were ~100  
247 ppb, dissolved in ~1 ml 2% HNO<sub>3</sub>. Isotopic analyses were carried out on a  
248 ThermoFinnigan Neptune MC-ICP-MS at the University of Bristol or a Neptune Plus at  
249 ETH Zürich, in low-resolution mode with introduction via a CPI PFA nebuliser (50  
250 µl/min) or a Savillex C-Flow PFA nebuliser (50 µl/min) attached to a glass spray chamber.  
251 Copper isotope ratios for samples were calculated using a standard bracketing approach by  
252 comparison to pure untreated NIST SRM 976 and are reported relative to this standard in  
253 delta-notation:

254

$$\delta^{65}\text{Cu} = 1000 \left[ \frac{(^{65}\text{Cu}/^{63}\text{Cu})_{\text{sample}}}{(^{65}\text{Cu}/^{63}\text{Cu})_{\text{SRM976}}} - 1 \right]$$

255

256 The long-term reproducibility of a secondary pure Cu standard was  $\delta^{65}\text{Cu} = +0.11 \pm$   
257  $0.11\text{‰}$  (n = 102) and  $+0.11 \pm 0.06\text{‰}$  (n = 112) at Bristol and ETH Zürich respectively,  
258 compared to  $+0.10 \pm 0.06\text{‰}$  measured at the Hebrew University (Asael et al., 2007). The

259 USGS reference materials BHVO-2, BIR-1A, BCR-2, and Nod P1 were analysed to assess  
260 accuracy. All uncertainties are given as 2 SD, unless stated otherwise.

261

## 262 **4. Results**

263

264 Accuracy and reproducibility of measured Cu and Al concentrations for two secondary  
265 standards – the commercially available SLRS-5 river standard from the National Research  
266 Council Canada and USGS Green River Shale SGR-1 – are reported in Table 2. Note that  
267 all Cu/Al ratios are given by mass, in ppm Cu/wt % Al (i.e.,  $\times 10^{-4}$ ). Copper isotope data for  
268 USGS reference materials are reported in Table 3. Values for BHVO-2, BIR-1A and BCR-  
269 2 fall within the ranges recommended in Moynier et al. (2017). Values obtained for Nod-  
270 P1 are consistent with that reported by Bigalke et al. (2010), and with the published mean  
271 for global Fe-Mn crusts and nodules  $+0.31 \pm 0.12\text{‰}$  (1SD, n=31; Data sources: Albarède,  
272 2004; Little et al., 2014a).

273

### 274 *4.1 Cu/Al ratios and Cu isotope data*

275 Down-core Cu/Al and  $\delta^{65}\text{Cu}_{\text{bulk}}$  data are presented graphically in Figures 2 – 5 and  
276 tabulated in full in the electronic supplementary material (ESM Table 1) and summarised  
277 in Table 4 (site-by-site averages). Where available, plotted isotope data are compared to  
278 mean values for proximal oxic sediments (Black Sea: oxic Station 16, Cariaco Basin: oxic  
279 section of core). In other locations, comparisons are made to the published average  
280 lithogenic Cu isotope composition ( $\delta^{65}\text{Cu}_{\text{lith}} = +0.08 \pm 0.17\text{‰}$ , 1 SD, n = 334; Moynier et  
281 al., 2017).

282

283 Aluminium is assumed to be immobile during diagenesis and is used as a tracer of the  
284 lithogenic component of the sediment. To accurately define the non-lithogenic sedimentary  
285 Cu component, measured Cu/Al ratios should ideally be compared to the Cu/Al ratio of  
286 local lithogenic background material (e.g., Böning et al., 2012; Little et al., 2015). In this  
287 study, the local background is taken as the minimum measured Cu/Al ratio from proximal  
288 oxic sediments where available (Black Sea, Cariaco Basin), following Böning et al. (2012).  
289 In the absence of an estimate for the local lithogenic background sedimentation in the  
290 California Borderland Basins, we compare Cu/Al ratios in Figure 4 with the most recent  
291 upper continental crust (UCC) estimate of  $3.5 \times 10^{-4}$  (Rudnick and Gao, 2003). The  
292 lithogenic background for sediments deposited close to Peru has previously been

293 approximated to that of a Peruvian andesite (Böning et al., 2004; Scholz et al., 2011; Little  
294 et al., 2015). A Cu/Al ratio of  $4.5 \times 10^{-4}$  can be calculated for average andesite from the  
295 Central Volcanic Zone of Peru (values derived from the GEOROC database of the Max-  
296 Planck Institute for Chemistry, Mainz, Germany; Sarbas and Nohl, 2009). A similar value  
297 of  $4.0 \times 10^{-4}$  can be calculated for a compilation of Trans Mexican Volcanic Belt samples  
298 (also derived from the GEOROC database). It is to this range of values ( $4.0 - 4.5 \times 10^{-4}$ )  
299 that samples from the Mexican and Peru margins are compared in Figure 5.

300

301 Elevated Cu/Al ratios compared to the (local) lithogenic background (Figures 2 – 5) are  
302 indicative of the presence of authigenic (chemically precipitated or scavenged) and/or  
303 biogenic (cellular and/or skeletal) Cu, which together are termed the ‘bioauthigenic’  
304 fraction (after Little et al., 2016). Note that the biogenic (or uptake-derived) component of  
305 Cu in the sediment is predicted to be small (<20%; Little et al., 2015), but that scavenging  
306 of Cu by particulate organic carbon is likely an important route by which Cu is delivered to  
307 the sediment.

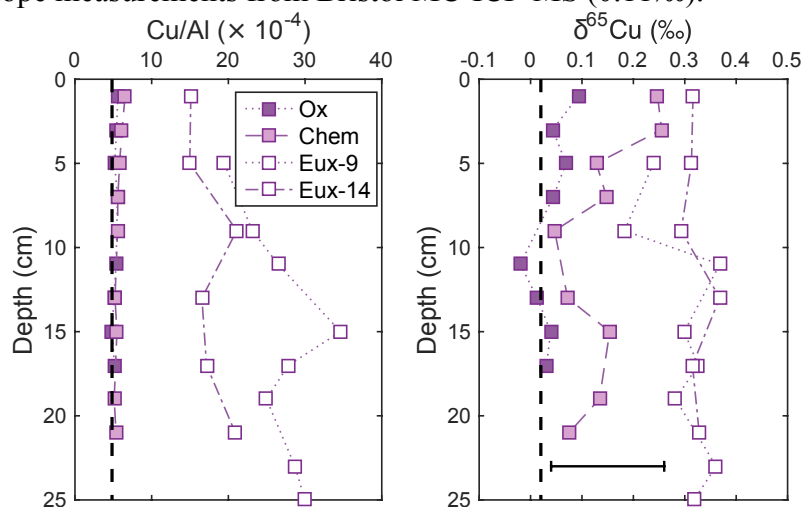
308

#### 309 *4.1.1 Black Sea*

310 Cu/Al and  $\delta^{65}\text{Cu}$  data for the four Black Sea sites are presented in Figure 2. Sediments  
311 from oxic Station 16 are assumed to represent the local lithogenic background  
312 sedimentation (mean Cu/Al =  $5.3 \pm 0.5 \times 10^{-4}$ , minimum Cu/Al =  $4.8 \times 10^{-4}$ ). In support of  
313 this assumption, these sediments have a lithogenic Cu isotope composition with an average  
314  $\delta^{65}\text{Cu}$  of  $+0.04 \pm 0.07\%$ . Chemocline Station 16B shows Cu/Al ratios (mean Cu/Al =  $5.7 \pm$   
315  $0.9 \times 10^{-4}$ ) very close to those of oxic Station 16, suggesting no significant bioauthigenic  
316 enrichment, except for the two surface-most samples (Cu/Al =  $6.5$  and  $6.1 \times 10^{-4}$  at 0 – 2  
317 cm and 2 – 4 cm respectively). However, despite dominantly lithogenic Cu/Al ratios,  
318 samples from Station 16B exhibit heavier and more variable  $\delta^{65}\text{Cu}$ , with an average of  
319  $+0.14 \pm 0.15\%$ . The two upper-most samples (both at  $+0.25\%$ ) again exhibit the greatest  
320 deviation from lithogenic values. The two euxinic stations 9 and 14 are indistinguishable  
321 and isotopically heavy compared to lithogenic Cu (Station 9:  $+0.30 \pm 0.12\%$ , Station 14:  
322  $+0.32 \pm 0.05\%$ ), despite slightly more elevated Cu/Al ratios at Station 9 compared to  
323 Station 14 (mean Cu/Al at Station 9 =  $26.9 \pm 9.2 \times 10^{-4}$  compared to  $17.6 \pm 5.5 \times 10^{-4}$  for  
324 Station 14). The mean  $\delta^{65}\text{Cu}$  for all Black Sea euxinic samples is  $+0.31 \pm 0.10\%$ .

325

326 **Figure 2.** Down-core Cu/Al and bulk  $\delta^{65}\text{Cu}$  data for the four Black Sea sites. Ox – Station  
 327 16, Chem – Station 16B, Eux-9 – Station 9, Eux-14 – Station 14. The local lithogenic  
 328 background, which is taken as the minimum Cu/Al and mean  $\delta^{65}\text{Cu}$  at oxic Station 16, is  
 329 given as a dashed black line. The error bar represents 2 SD external reproducibility on Cu  
 330 isotope measurements from Bristol MC-ICP-MS (0.11‰).



331

332

#### 333 4.1.2 Cariaco Basin

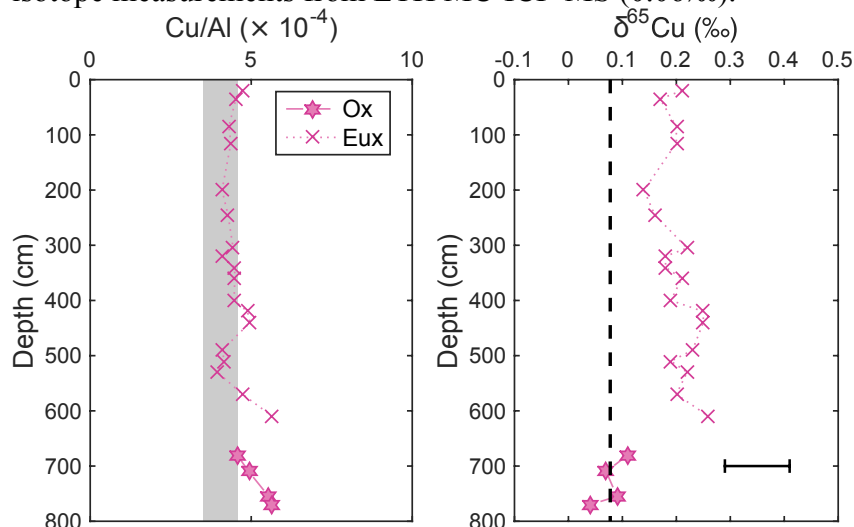
334 Cu/Al and  $\delta^{65}\text{Cu}$  data for the Cariaco Basin drill-core samples are presented in Figure 3.

335 The lowermost four samples represent deposition under oxic conditions linked to the sea-  
 336 level low stand of the last glacial period (Lyons et al., 2003). These four oxic samples have  
 337 a lithogenic  $\delta^{65}\text{Cu}$  of  $+0.08 \pm 0.06\text{‰}$  and an average Cu/Al ratio of  $5.2 \pm 1.0 \times 10^{-4}$ , which  
 338 is elevated compared to average UCC (at  $3.1 - 3.5 \times 10^{-4}$ ). The euxinic (interglacial)  
 339 sediments have a lower average Cu/Al ratio ( $4.5 \pm 0.8 \times 10^{-4}$ ) and significantly heavier Cu  
 340 isotope values compared to those deposited under oxic conditions, with a mean  $\delta^{65}\text{Cu} =$   
 341  $+0.20 \pm 0.06\text{‰}$ . If the four oxic samples are assumed to represent the local lithogenic  
 342 input, euxinic sediments in the Cariaco Basin show no bioauthigenic enrichment in Cu  
 343 over the lithogenic background value (Fig. 3).

344

345

346 **Figure 3.** Down-core Cu/Al and bulk  $\delta^{65}\text{Cu}$  data for the Cariaco Basin core. Lowermost  
 347 four samples (filled stars, ‘Ox’) were deposited during the last glacial period, under oxic  
 348 conditions. The remainder of the sediment core was deposited during the present  
 349 interglacial, when the water column was euxinic (crosses, ‘Eux’). The grey bar represents a  
 350 range of possible lithogenic Cu/Al ratios (including UCC and the local oxic minimum from  
 351 the glacial period samples). The dashed line represents global mean lithogenic  $\delta^{65}\text{Cu}$   
 352 (Moynier et al., 2017). The error bar represents 2 SD external reproducibility on Cu  
 353 isotope measurements from ETH MC-ICP-MS (0.06‰).



354

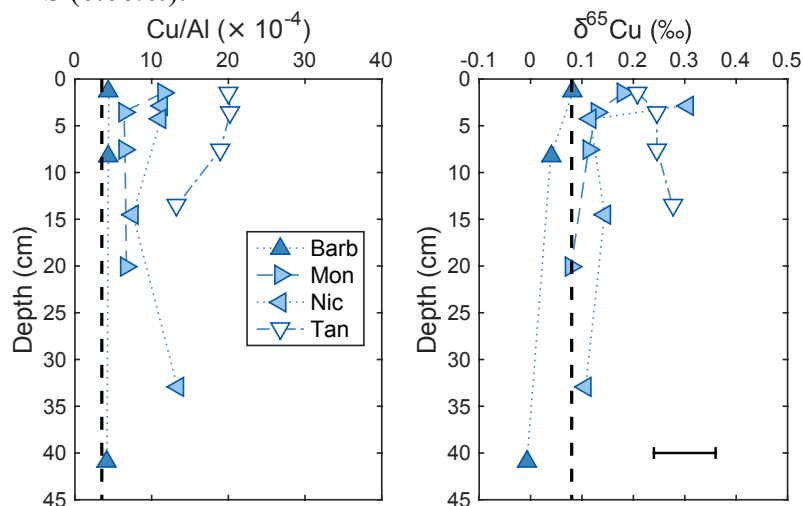
355

#### 356 4.1.3 California Borderland Basins

357 The most reducing of the four California Borderland sites, Santa Barbara, exhibits little or  
 358 no bioauthigenic enrichment of Cu (mean Cu/Al =  $4.5 \pm 0.8 \times 10^{-4}$ ) with  $\delta^{65}\text{Cu}$  values  
 359 ( $\delta^{65}\text{Cu} = +0.04 \pm 0.09\text{‰}$ ) that are unfractionated from lithogenic values. Santa Monica  
 360 Basin, which has ferruginous porewaters, exhibits higher Cu/Al ratios and slightly  
 361 isotopically heavy Cu, particularly the surface-most sample (Cu/Al at 1.5 cm =  $11.4 \times 10^{-4}$   
 362 cf. mean Cu/Al at depths >1.5 cm =  $6.5 \pm 0.3 \times 10^{-4}$ ;  $\delta^{65}\text{Cu}$  at 1.5 cm =  $+0.18\text{‰}$  cf. mean  
 363  $\delta^{65}\text{Cu}$  >1.5 cm =  $+0.11 \pm 0.05\text{‰}$ ; Fig. 4). Note that an anthropogenic source of metals has  
 364 been identified at this site, and this may contribute to the enrichment observed in the  
 365 surface 1 – 2 cm (Finney and Huh, 1989; Bruland et al., 1994). San Nicolas, where  
 366 porewaters can be defined as manganoous, also has a surface-most sample that is  
 367 isotopically heavier than the remainder of the sediment core (at  $+0.31\text{‰}$  versus  $+0.12 \pm$   
 368  $0.04\text{‰}$ ; Fig. 4). Copper throughout this core is significantly enriched (mean Cu/Al =  $10.9 \pm$   
 369  $4.8 \times 10^{-4}$ ) relative to UCC. The most Cu enriched of the California Borderland Basin sites  
 370 is Tanner Basin. Mean Cu/Al ratios at this site are  $18.1 \pm 6.5 \times 10^{-4}$  and Cu is isotopically  
 371 heavy compared to lithogenic Cu at  $+0.24 \pm 0.06\text{‰}$ .

372

373 **Figure 4.** Down-core Cu/Al and bulk  $\delta^{65}\text{Cu}$  data for the California Borderland basins. Barb  
 374 – Santa Barbara basin, Mon – Santa Monica basin, Nic – San Nicolas basin, Tan – Tanner  
 375 basin. Estimates of the lithogenic background (UCC Cu/Al: Rudnick and Gao, 2003;  
 376 global mean lithogenic  $\delta^{65}\text{Cu}$ ; Moynier et al., 2017) are given as a dashed black line. Error  
 377 bar represents 2 SD external reproducibility on Cu isotope measurements from ETH MC-  
 378 ICP-MS (0.06‰).



379  
 380

#### 381 4.1.4 Mexican and Peru Margins

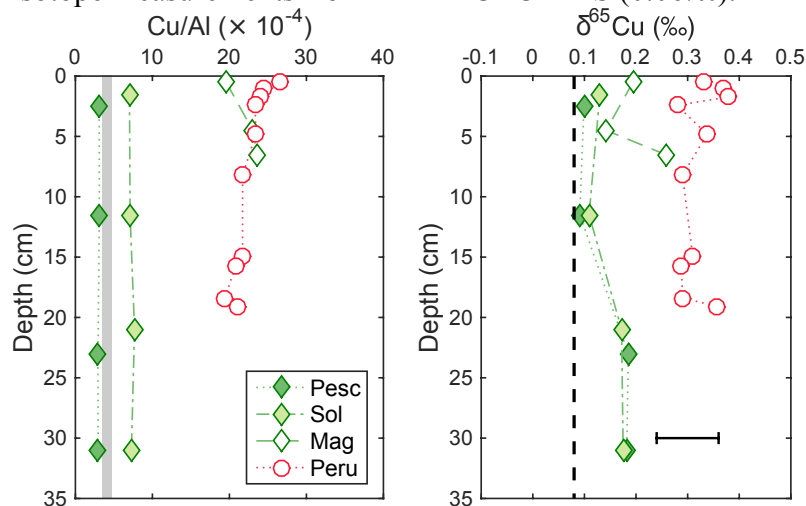
382 The Peru margin exhibits the highest absolute Cu concentrations of any of the sites  
 383 analysed here (up to 75 ppm). Enrichment is greatest close to the sediment surface and  
 384 declines with depth (Fig. 5; mean Cu/Al =  $22.6 \pm 4.2 \times 10^{-4}$ ). Copper isotope values at this  
 385 site are homogeneous with depth and isotopically heavy compared to the lithogenic  
 386 baseline ( $\delta^{65}\text{Cu} = +0.32 \pm 0.07\text{‰}$ ; Fig. 5).

387

388 The Magdalena and Peru margin sites are similar in their Cu geochemistry. The Magdalena  
 389 margin also exhibits high Cu/Al ratios ( $22.1 \pm 4.4 \times 10^{-4}$ ) and isotopically heavy  $\delta^{65}\text{Cu}$   
 390 ( $+0.20 \pm 0.12\text{‰}$ ). By contrast, the sites of Soledad Basin (Cu/Al =  $7.3 \pm 0.6 \times 10^{-4}$ ) and  
 391 Pescadero Slope (Cu/Al =  $3.0 \pm 0.2 \times 10^{-4}$ ) are only moderately elevated or not enriched (or  
 392 even slightly depleted), respectively. These two sites are isotopically indistinguishable and  
 393 exhibit slightly heavier Cu isotope values compared to typical lithogenic signatures  
 394 (Soledad:  $+0.15 \pm 0.06\text{‰}$ ; Pescadero:  $+0.14 \pm 0.10\text{‰}$ ).

395  
 396

397 **Figure 5.** Down-core Cu/Al and bulk  $\delta^{65}\text{Cu}$  data for the Mexican and Peru margin sites.  
 398 Pesc – Pescadero slope, Sol – Soledad basin, Mag – Magdalena margin, Peru – Peru  
 399 margin. Grey bar gives range of Peruvian andesite-Mexican volcanic zone Cu/Al ratios,  
 400 see text in section 4.1 for details. Dashed black line represents global mean lithogenic  
 401  $\delta^{65}\text{Cu}$  (Moynier et al., 2017). Error bar represents 2 SD external reproducibility on Cu  
 402 isotope measurements from ETH MC-ICP-MS (0.06‰).



403  
 404

## 405 5. Discussion

406

### 407 5.1 Covariation of $\delta^{65}\text{Cu}$ and Al/Cu in marine sediments

408

409 As a whole, the dataset presented here shows limited variability in  $\delta^{65}\text{Cu}$  values, from –  
 410 0.02‰ to +0.37‰. For comparison, the measured range in  $\delta^{65}\text{Cu}$  found for typical Earth  
 411 surface materials spans approximately –1.5‰ to +2‰ (e.g., Moynier et al., 2017), though  
 412 this range is extended considerably with the inclusion of Cu-bearing ore minerals (–16.5‰  
 413 to +10.0‰; Mathur et al., 2009).

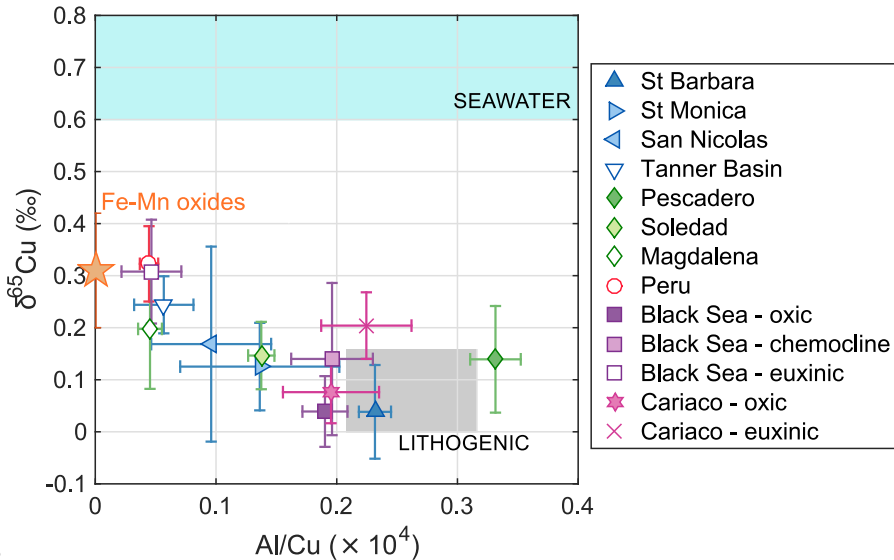
414

415 All samples from this study are isotopically lighter than data for the dissolved phase in  
 416 seawater (at +0.6 to +0.9‰, Fig. 6; Vance et al., 2008; Thompson et al., 2014; Takano et  
 417 al., 2014). A negative correlation (Fig. 6;  $R^2_{\text{all data}} = 0.40$ ,  $p < 0.001$ ) is observed between  
 418  $\delta^{65}\text{Cu}$  values and Al/Cu ratios. This relationship can be explained, to a first order, by  
 419 mixing of two distinct end-member sources of Cu. The first is a lithogenic source, with a  
 420 high Al/Cu ratio and a lithogenic Cu isotope composition of ~0 to +0.1‰ (grey box, Fig.  
 421 6). The second mixing component can be termed the bioauthigenic Cu end member. It has  
 422 a low Al/Cu ratio and an isotope composition of about +0.3‰. While the presence of a  
 423 lithogenic end member is intuitive, the fact that just one other component can explain a

424 significant fraction of the variability in the remainder of the dataset is unexpected and  
 425 merits further discussion.

426

427 **Figure 6.** Covariation of  $\delta^{65}\text{Cu}$  with Al/Cu in marine sediments. Each site is represented  
 428 by its mean  $\delta^{65}\text{Cu}$  and Al/Cu values  $\pm 2$  SD error bars. Symbols for each site are the same  
 429 as in Figures 2 – 5. The range of estimated bulk seawater isotopic compositions (+0.6 to  
 430 +0.9‰) is shown as a shaded blue bar. The range and mean of lithogenic Al/Cu values and  
 431  $\delta^{65}\text{Cu}$  ratios are shown as a grey box. For comparison, the mean and 1 SD of the surface  
 432 layers of global Fe-Mn oxide sediments is shown as an orange star.



433

434 The isotope composition of the bioauthigenic Cu component of the sediment can be  
 435 calculated for individual samples by mass balance, assuming a Cu/Al ratio and  $\delta^{65}\text{Cu}$  value  
 436 of the lithogenic background material ( $\text{Cu}/\text{Al}_{\text{lith}}$  and  $\delta^{65}\text{Cu}_{\text{lith}}$ ). First, the lithogenic fraction  
 437 ( $X_{\text{lith}}$ ) of the total Cu is calculated:

438

$$439 \quad X_{\text{lith}} = \frac{\frac{\text{Cu}}{\text{Al}_{\text{lith}}} \times \text{Al}_{\text{sample}}}{\text{Cu}_{\text{sample}}},$$

440

441 where  $\text{Al}_{\text{sample}}$  and  $\text{Cu}_{\text{sample}}$  are the measured bulk Al and Cu concentrations of the sample.

442 The bioauthigenic  $\delta^{65}\text{Cu}_{\text{auth}}$  value can then be calculated:

443

$$444 \quad \delta^{65}\text{Cu}_{\text{auth}} = \frac{(\delta^{65}\text{Cu}_{\text{bulk}} - \delta^{65}\text{Cu}_{\text{lith}} \cdot X_{\text{lith}})}{X_{\text{auth}}},$$

445

446 where  $\delta^{65}\text{Cu}_{\text{bulk}}$  is the measured  $\delta^{65}\text{Cu}$  ratio of the sample, and  $X_{\text{auth}}$  is the fraction of  
 447 bioauthigenic Cu (i.e.,  $X_{\text{auth}} = 1 - X_{\text{lith}}$ ). This calculation is straightforward but gives  
 448 unreasonable values when the lithogenic fraction is very large (>90%). This situation

449 applies to the Cariaco Basin, the Santa Barbara Basin, and the Pescadero Slope sites, which  
450 all show little or no bioauthigenic enrichment. Excluding these three sites, and assuming  
451 lithogenic  $\text{Cu}/\text{Al}_{\text{lith}}$  and  $\delta^{65}\text{Cu}_{\text{lith}}$  values for the remaining sites as detailed in section 4.1, the  
452 calculated bioauthigenic end member has a Cu isotope composition of  $+0.31 \pm 0.11\%$  (1  
453 SD,  $n = 43$ ; see ESM Table 1 for sample-by-sample calculated  $\delta^{65}\text{Cu}_{\text{auth}}$  values). Exclusion  
454 of the Black Sea data yields a margin-only  $\delta^{65}\text{Cu}_{\text{auth}}$  of  $+0.28 \pm 0.11\%$  (1 SD,  $n = 29$ ).  
455 Note that using a single  $\text{Cu}/\text{Al}_{\text{lith}}$  value for all sites and varying this ratio between 3.0 and  
456  $4.5 \times 10^{-4}$  alters the calculated  $\delta^{65}\text{Cu}_{\text{auth}}$  by less than  $\pm 0.02\%$ . The calculation is somewhat  
457 more sensitive to the assumed  $\delta^{65}\text{Cu}_{\text{lith}}$  value. Taking the published mean  $\delta^{65}\text{Cu}_{\text{lith}} \pm 1$  SD  
458 (where  $\delta^{65}\text{Cu}_{\text{lith}} = 0.08 \pm 0.17\%$ ; Moynier et al., 2017) – i.e. using a range for  $\delta^{65}\text{Cu}_{\text{lith}}$  of –  
459 0.09 to  $+0.25\%$  – gives a range in the calculated mean  $\delta^{65}\text{Cu}_{\text{auth}}$  of  $+0.39$  to  $+0.23\%$ .

460

461 The calculated bioauthigenic end member isotope composition of about  $+0.3\%$  closely  
462 corresponds to observed values for the surface layers of Fe-Mn crusts and nodules (orange  
463 star in Fig. 6; mean  $\delta^{65}\text{Cu}_{\text{Fe-Mn oxides}} = +0.31 \pm 0.12\%$ , 1SD,  $n = 31$ , data sources: Albarède,  
464 2004; Little et al., 2014a). Fe-Mn crusts have previously been used as an analogue for the  
465 dispersed Fe-Mn oxide phases found throughout deep-sea pelagic sediments that are  
466 thought to be responsible for Cu removal from the ocean under normal ‘oxic’ marine  
467 conditions (Little et al., 2014a). Somewhat surprisingly, therefore, the data presented here  
468 suggest that Cu is removed from the ocean with a homogeneous isotopic composition (of  
469 about  $+0.3\%$ ) in all oceanic settings. Particularly surprising is the observation that, despite  
470 near quantitative removal of Cu from the sulphidic water columns of the Black Sea and  
471 Cariaco Basin (Jacobs et al., 1987; Haraldsson and Westerlund, 1991; Tankéré et al.,  
472 2001), bioauthigenic Cu isotope values from these two basins do not appear to record the  
473  $\delta^{65}\text{Cu}$  of global mean seawater (at  $+0.6$  to  $+0.9\%$ ; Vance et al., 2008; Thompson et al.,  
474 2014; Takano et al., 2014). We return to this observation in section 5.3.

475

### 476 *5.2 Bioauthigenic Cu in sediments: the isotopic counterpart to strong organic ligand-* 477 *bound Cu in the dissolved pool?*

478

479 The vast majority of dissolved copper in all aqueous environments, from rivers and their  
480 estuaries (e.g., Dryden et al., 2004; Laglera and Van den Berg, 2003) to the open ocean  
481 (e.g., Coale and Bruland, 1988, 1990; Moffett et al., 1990; Lucia et al., 1994; Leal and Van  
482 den Berg, 1998; Moffett and Dupont, 2007; Jacquot and Moffett, 2015), is complexed to

483 strong organic ‘L1-type’ ligands, which have binding constants (log K) in the range of  
484 about 12–16. Both *ab initio* calculations (Sherman, 2013) and experiments (Bigalke et al.,  
485 2010; Ryan et al., 2014) indicate that strong organic ligands preferentially complex the  
486 heavy Cu isotope. Isotopically heavy Cu in the dissolved pool of rivers and the ocean has  
487 thus previously been hypothesised to result from preferential complexation of heavy Cu  
488 isotopes by these strong organic ligands (Vance et al., 2008; Thompson et al., 2014; Little  
489 et al., 2014b). Specifically, Vance et al. (2008) proposed that an equilibrium fractionation  
490 occurs directly between an organically complexed dissolved pool and the surface of  
491 scavenging particles (Vance et al., 2008). This scenario could also be invoked to explain  
492 the homogenous composition of the bioauthigenic Cu output flux observed here. The  
493 homogeneous composition of the oceanic Cu sink would, in this case, require open system  
494 steady-state fractionation with a fractionation factor ( $\Delta = \delta^{65}\text{Cu}_{\text{seawater}} - \delta^{65}\text{Cu}_{\text{sinks}}$ ) of  
495  $\sim 0.4\text{‰}$  between the aqueous and particulate phase.

496

497 Another plausible explanation for the homogeneous isotopic composition of the  
498 bioauthigenic Cu output flux, regardless of *sedimentary* redox state, is that an equilibrium  
499 isotopic fractionation exists between two species in the oxygenated *aqueous* phase. First,  
500 the organically complexed pool is highly soluble and enriched in heavy isotopes due to the  
501 strong binding environment provided by the strong organic ligands. Second, a particle  
502 reactive free  $\text{Cu}^{2+}$  pool, which is  $\sim 0.4\text{‰}$  lighter than the organic ligand-bound pool, is  
503 scavenged to particulates. Consistent with this scenario, Ryan et al. (2014) measured an  
504 isotopic fractionation factor  $\Delta_{\text{ligand-free}} = 0.44 \pm 0.40 \text{‰}$  ( $n = 3$ , 2SD) for a synthetic ligand  
505 (NTA) with a similar log K to natural L1-type ligands ( $\log K_{\text{NTA}} = 14.4$ ). In this case,  
506 where fractionation occurs between two Cu species in the aqueous phase, the nature of the  
507 particulate material to which Cu is scavenged is not relevant to the isotopic fractionation  
508 expressed. In the alternative scenario, where an equilibrium fractionation exists between  
509 the aqueous and particulate pools, there would need to be a near constant fractionation  
510 factor between aqueous Cu and all potential scavenging surfaces.

511

512 In either scenario, we hypothesise that scavenging by particulate organic matter plays a key  
513 role in the water column. If this scavenging is a reversible process (e.g., Little et al., 2013),  
514 and exchange continues with the dissolved pool as particles sink, then bottom water  
515 isotope compositions will determine the isotope composition of particles when they reach  
516 the sediment. In turn, this process may contribute to the homogeneity of the output flux,

517 because deep waters exhibit less isotopic variability than the upper water column (Vance et  
518 al., 2008; Takano et al., 2014, Thompson et al., 2014). Scavenging associated with Fe-Mn  
519 cycling either in the water column or within the sediment is also likely to be important,  
520 dependent on the setting. For example, active Fe-Mn oxide cycling close to the sediment-  
521 water interface (e.g., San Nicolas, Santa Monica; Fig. 4) appears to enhance fixation of Cu  
522 with the bioauthigenic  $\delta^{65}\text{Cu}$  signature. Detailed spectroscopic and experimental work at  
523 the mineral-organic-water interface increasingly supports the suggestion that organic and  
524 oxide-bound phases are often inextricably linked (Lalonde et al., 2012; Johnson et al.,  
525 2015; Tribovillard et al., 2015). In the case of an equilibrium isotope fractionation between  
526 the dissolved phase and scavenging particles, this organic-oxide linkage may also  
527 contribute to the isotopic homogeneity of the sedimentary sink.

528

### 529 *5.3 Cu in euxinic settings*

530

#### 531 *5.3.1 The Cariaco Basin*

532 Near quantitative removal of Cu is observed from the euxinic water columns of both the  
533 Black Sea and Cariaco Basin (Haraldsson and Westerlund, 1991; Tankéré et al., 2001;  
534 Jacobs et al., 1987). Despite this removal from the water column, we do not observe  
535 significantly elevated Cu/Al in Cariaco Basin sediments (Fig. 3). There is, however, a shift  
536 in  $\delta^{65}\text{Cu}$  ratios across the oxic-anoxic transition of the sediment core, from about +0.08 in  
537 the oxic interval to +0.20‰ in the euxinic interval (Fig. 3). Given the absence of  
538 appreciable Cu enrichment, one possible explanation of this isotopic shift is a change in the  
539 isotope composition of the local lithogenic background material. A change in the source of  
540 lithogenic material to the Cariaco Basin on glacial-interglacial timescales has previously  
541 been proposed based on Al/Ti ratios. This change is hypothesised to reflect an increased  
542 supply of Ti-rich dust from the Sahara during glacial periods, due to the more southerly  
543 position of the ITCZ (Yarincik et al., 2000; Martinez et al., 2010). Alternatively, the data  
544 and their uncertainties do permit the presence of a small amount of bioauthigenic Cu in the  
545 euxinic interval. For example, assuming an UCC Cu/Al ratio of  $3.5 \times 10^{-4}$  (Note: this ratio  
546 is lower than that observed in the oxic interval), and  $\delta^{65}\text{Cu}_{\text{lith}}$  of +0.08‰, the mean  
547 calculated  $\delta^{65}\text{Cu}_{\text{auth}}$  for the euxinic portion of the sediment pile is  $+0.66 \pm 0.25\%$ , similar  
548 to that of modern open ocean seawater  $\delta^{65}\text{Cu}$  (at approximately +0.7‰). There is an  
549 indication, therefore, that bioauthigenic Cu deposited in sediments under Cariaco Basin-  
550 type hydrographic conditions, where euxinia is primarily driven by productivity without

551 strong basin restriction, may indeed record open ocean  $\delta^{65}\text{Cu}$ . However, due to the very  
552 low Cu enrichment observed (see also section 5.4), the local lithogenic background must  
553 be carefully characterised and corresponding calculated  $\delta^{65}\text{Cu}_{\text{auth}}$  values should be  
554 interpreted with caution.

555

### 556 *5.3.2 The Black Sea*

557 Copper is enriched by a factor of 3 to 7 in sediments from the Black Sea euxinic stations  
558 compared to those from the oxic stations (Fig. 2), such that the assumed composition of the  
559 local lithogenic background has very little impact on calculated  $\delta^{65}\text{Cu}_{\text{auth}}$  values (unlike in  
560 the Cariaco Basin). The Black Sea Cu isotope data therefore present us with a puzzle:  
561 given near quantitative removal from the water column, why are the  $\delta^{65}\text{Cu}$  values of  
562 euxinic Black Sea sediments not more similar to the isotopic composition of mean global  
563 seawater (at approximately +0.7‰)? Instead we find that the Black Sea bioauthigenic Cu  
564 has an isotope composition that is similar to the remainder of the reducing sedimentary  
565 dataset presented here (i.e., at around +0.3‰).

566

567 One possibility is that the Cu isotope composition of the upper water column of the  
568 Mediterranean, which supplies the Black Sea through the shallow Bosphorus Strait between  
569 13 and 110 m water depth, is isotopically lighter than that of mean global seawater.  
570 Although Cu isotope data for seawater remains relatively sparse, the data that exist show  
571 limited variability in deep waters (at +0.6 to 0.9‰: Vance et al., 2008; Takano et al., 2014;  
572 Thompson et al., 2014), but frequent small deviations towards lighter  $\delta^{65}\text{Cu}$  values in the  
573 upper water column (down to +0.4 to 0.5‰: Takano et al., 2014). These relatively light  
574 surface values are most easily explained as the result of the deposition of aerosol dust, and  
575 the Mediterranean does receive a high mineral dust flux from the Sahara (Prospero, 1996).  
576 However, assuming modern inflow through the Bosphorus Strait of  $305 \text{ km}^3 \text{ yr}^{-1}$  (Özsoy  
577 and Ünlüata, 1997), and a surface water Cu concentration in the Mediterranean of 2.5  
578 nM (Saager et al., 1993), the magnitude of the Mediterranean Cu source is about  $7 \times 10^7 \text{ g}$   
579  $\text{yr}^{-1}$ . The mean calculated authigenic Cu content of euxinic Black Sea sediments is ~35  
580 ppm (ESM Table 1, range: 28 – 48 ppm). Given this value, and assuming a sediment  
581 density of  $2.3 \text{ g cm}^{-3}$ , porosity of 80%, anoxic basin area of  $318,582 \text{ km}^2$  and a  
582 sedimentation rate of  $0.0155 \text{ cm yr}^{-1}$ , we calculate a Cu output flux to Black Sea euxinic  
583 sediments of  $8 \times 10^8 \text{ g yr}^{-1}$ . This estimate is an order of magnitude higher than the  
584 estimated Mediterranean input flux. This imbalance is exacerbated by the fact that there is

585 also a return flux to the Mediterranean from the surface Black Sea, representing a further  
586 substantial output of Cu from the basin. Hence, input of Cu from the Mediterranean alone  
587 can explain neither the enrichment nor the isotope signature of Cu observed in Black Sea  
588 sediments.

589

590 Rivers are the other likely key input of Cu to the Black Sea. The previously measured  
591 range of  $\delta^{65}\text{Cu}$  in a subset of relatively pristine global rivers is +0.02 to +1.45‰, with a  
592 discharge-weighted average of +0.68‰ (Vance et al., 2008). A measurement of Black Sea  
593 surface water of +0.92‰ (Table 5; for sample collection and pre-concentration techniques,  
594 see Vance et al., 2016a) is within this riverine range and the range of published open ocean  
595 values. Though the isotope composition of the Black Sea surface ocean may be  
596 anthropogenically perturbed (e.g., Vance et al., 2016a), it seems unlikely – though we  
597 cannot definitively rule it out – that the relatively light isotopic composition of Black Sea  
598 sediments is a direct result of supply of isotopically light Cu from rivers.

599

600 A plausible explanation for the coherent isotopic composition of Black Sea sediments  
601 versus those from other marine settings is that the source of Cu to the restricted deep basin  
602 has, in fact, been subject to biogeochemical cycling similar to that envisaged in section 5.2.  
603 In this view, rivers supply isotopically heavy Cu to the oxic Black Sea surface layer. The  
604 transfer of this Cu to the deep euxinic portion of the basin is then mediated by the cycling  
605 of Fe and Mn and is associated with an isotopic fractionation between the aqueous and  
606 particulate phase similar to that which is proposed for the open ocean. Copper is  
607 complexed by organic ligands in Black Sea surface waters (Muller et al., 2001), and  
608 significant cycling of trace metals across the redoxcline has been hypothesised associated  
609 with the cycling of nanoparticulate Fe and Mn oxides at this depth (e.g., Lyons and  
610 Severmann, 2006; Little et al., 2015; Vance et al., 2016a). Specifically, nanoparticulate Fe  
611 and Mn oxides may form following their efflux from shelf sediments. These  
612 nanoparticulate phases can then be transported to the basin interior, where they are re-  
613 reduced and dissolve: this is a version of the *benthic redox shuttle* (Severmann et al., 2008;  
614 Scholz et al., 2013; 2014). These Fe-Mn nanoparticles sorb other trace metals, forming a  
615 fine particle layer at the redoxcline that is rich in Cu, Ni, Zn, and other metals (Tankéré et  
616 al., 2001). The scavenged Cu, which need not be shelf-sediment sourced (as invoked for Fe  
617 and Mn), is then released to the euxinic portion of the basin on reduction of the host Fe-Mn  
618 nanoparticles. Once there, sulphide minerals quantitatively re-scavenge the supplied Cu. In

619 this view, the ‘shuttled’ Cu would have an isotope composition of the bioauthigenic end  
620 member at +0.3‰, i.e., approximately +0.6‰ lighter than organically complexed,  
621 isotopically heavy, residual Cu in modern Black Sea surface waters.

622

623 Some support for this hypothesis comes from chemocline site 16B. Here, the upper two  
624 data points (upper 4 cm of core) are slightly enriched in Cu and are distinctly isotopically  
625 heavy at +0.25‰ – similar to the bioauthigenic end member – compared to lithogenic-like  
626  $\delta^{65}\text{Cu}$  values observed deeper in the core (Fig. 2). The sediments at Station 16B were  
627 deposited close to the position of the redoxcline at the time of coring, with dissolved  
628 oxygen at trace levels (Lyons, 1991). Enrichments in AVS (acid volatile sulphur) were  
629 evident in the black-grey, banded upper 2-4 cm of the core, compared to the increasingly  
630 bioturbated grey layers below. These observations have been interpreted to reflect an  
631 evolution from a more to a less oxygenated environment at this site (Lyons, 1991), i.e., a  
632 shoaling of the redoxcline, an assertion that is supported by the  $\delta^{65}\text{Cu}$  data presented here.

633

#### 634 *5.4 The lithogenic dilution effect on Cu enrichment in marine sediments*

635

636 Cu/Al data from the Cariaco Basin highlight that anoxia, and even euxinia, is not by itself  
637 sufficient to produce strong authigenic Cu enrichments in sediments. Other data presented  
638 here also illustrate this point clearly: the most reducing sedimentary environment of the  
639 California Borderland basins is the Santa Barbara basin, which shows no authigenic Cu  
640 enrichment and a lithogenic isotope composition. In Figure 7 we highlight one key reason  
641 for this, the control on Cu enrichment by sediment accumulation rate.

642

643 To isolate the role of lithogenic dilution of Cu contents in marine sediments, Al  
644 accumulation rates ( $S_{\text{Al}}$ ) were calculated using estimates of sediment accumulation rates  
645 from the literature, summarised in Table 1, and measured Al concentrations from this  
646 study. Significant Cu enrichment is observed only at sites with an  $S_{\text{Al}}$  of considerably less  
647 than  $0.1 \text{ mg cm}^{-2} \text{ yr}^{-1}$  (Fig. 7). Plotting the  $S_{\text{Al}} - \text{Al/Cu}$  relationship in this way allows a  
648 quantitative assessment of the lithogenic dilution effect on Cu enrichment, via a box model  
649 approach outlined by Jacobs et al. (1985; 1987). Full details of the box model are given in  
650 the ESM. In brief, it is assumed that the flux of Cu (or any metal) to the sediment is  
651 comprised of two components, the relative magnitude of which will determine metal  
652 enrichment in the sediment: (1) a detrital (or lithogenic) flux defined by the Cu/Al ratio of

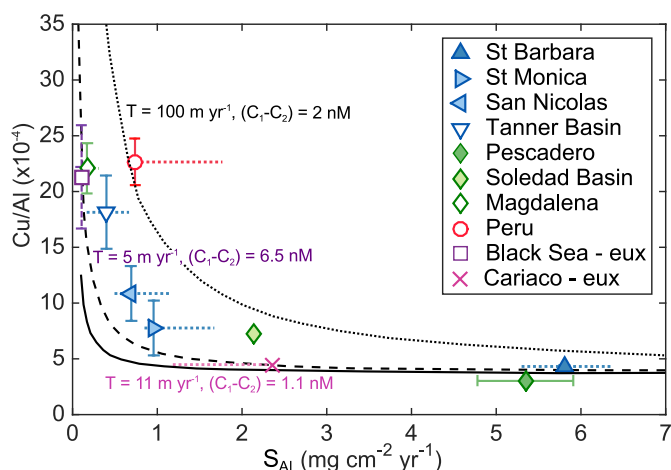
653 upper continental crust  $(\text{Cu}/\text{Al})_{\text{lith}}$  and the accumulation rate of Al ( $S_{\text{Al}}$ ) and (2) a  
654 bioauthigenic flux derived from removal of dissolved Cu from the water column. We  
655 assume that the latter may reflect either sulphidisation or uptake/scavenging by particulate  
656 organic carbon and/or Fe-Mn oxides. The model is made up of an oxic surface ocean box  
657 (Box 1) and an anoxic deep water box (Box 2), each of which are well mixed and exchange  
658 on a timescale,  $T$ , in  $\text{m yr}^{-1}$  (ESM Fig. 1). The authigenic enrichment of a metal,  $S_{\text{enrich}}$ ,  
659 then depends on three parameters: (1)  $S_{\text{Al}}$ ; (2) the concentration difference between oxic  
660 box 1 and anoxic box 2,  $C_1-C_2$ ; and (3) the timescale of mixing,  $T$ . We apply this model to  
661 the Cariaco Basin (directly following Jacobs et al., 1987) and to the Black Sea. Parameters  
662 used are given in Table 6. Note that  $T$  is related to the residence time of water in the deep  
663 box,  $\tau_2$ , by the thickness of this box,  $z_2$ :  $T = z_2\tau_2^{-1}$ . This mixing timescale is somewhat  
664 slower in the Black Sea ( $\sim 5 \text{ m yr}^{-1}$ ) than in the Cariaco Basin ( $\sim 11 \text{ m yr}^{-1}$ ), due to the  
665 longer residence time of Black Sea deep waters (Table 6). In addition, the parameter  $C_1-C_2$   
666 in the Black Sea (6.5 nM; Tankéré et al., 2001) is quadruple that of the Cariaco Basin (1.1  
667 nM, Jacobs et al., 1987), due to the relatively low Cu concentration of the South Atlantic  
668 source waters that flow into the Cariaco Basin. The results of the model are plotted as  
669 dashed (Black Sea model parameters) and solid (Cariaco Basin model parameters) black  
670 lines in Figure 7 for the full range of  $S_{\text{Al}}$  values observed for sites in this study. Agreement  
671 between the model and site-averaged Cu/Al values is observed for the two euxinic sites.

672

673 This simple 2-box model is not directly applicable to open margin sites, like the Peru and  
674 Magdalena margin regions, and we have insufficient data to perform a detailed analysis for  
675 the other basinal sites included here. We can, however, find parameters that give  
676 reasonable results, even for the exceptional Peru margin site (dotted black line, Fig. 7). For  
677 this model we assume a removal term of Cu into particulate organic matter of 2 nM, over a  
678 depth range of 100 m, and with a very short water residence time (1 year). This result  
679 should be considered illustrative only, nevertheless, the model gives clear mechanistic  
680 insight into lithogenic dilution of the bioauthigenic flux of Cu.

681

682 **Figure 7.** Al accumulation rate ( $S_{Al}$ ) versus site average Cu/Al. Black lines show  
 683 superimposed box model results (solid – Cariaco Basin; dashed – Black Sea; dotted – Peru  
 684 margin; see Table 6 for selected model parameters and ESM for additional model details).  
 685 All symbols are the same as in Figs 2 – 5. Coloured dotted ranges in  $S_{Al}$  reflect published  
 686 range in sediment accumulation rates for nearby sites compiled from the literature (see  
 687 Table 1). Error bars on Cu/Al ratios and  $S_{Al}$  (where sediment accumulation rates for the  
 688 same sediment core have been published) reflect 2 SD variability for the core.  
 689



690  
 691  
 692

### 693 5.5 Implications for Cu oceanic mass balance: a missing isotopically light Cu source

694

695 One of the motivations for this study was to place constraints on the modern reducing  
 696 sedimentary sink for Cu and Cu isotopes. A first order approximation of the net flux of Cu  
 697 into continental margin settings can be calculated using an estimate of marine organic C  
 698 burial rate and the slope of the  $C_{org}/Al$  versus Cu/Al relationship for continental margin  
 699 sites. This slope is 0.00041 g Cu/g C (ESM Fig. 3; data from this study and Böning et al.,  
 700 2012). Smith et al. (2015) calculate a global marine  $C_{org}$  burial rate of  $\sim 170 \times 10^{12}$  g C yr<sup>-1</sup>.  
 701 Together, this equates to an organic C associated Cu burial flux of  $\sim 11 \times 10^8$  mol yr<sup>-1</sup>. This  
 702 value is an order of magnitude higher than an estimate for the role of continental margin  
 703 sediments based on Mo as an analogue (Little et al., 2015) and slightly above the range of  
 704 Cu removal estimates to oxic pelagic sedimentary settings, estimated at  $1.6 - 9.7 \times 10^8$   
 705 mol/yr (Little et al., 2014a; Little et al., 2015). The calculation excludes the additional flux  
 706 of Cu to euxinic sediments via the redox-shuttle mechanism proposed for the Black Sea,  
 707 which is quantitatively small today ( $\sim 0.5 \times 10^8$  mol/yr; Little et al., 2015), but may have  
 708 been more significant in the past. Given a total ocean Cu budget of  $4.2 \times 10^{12}$  moles (Little  
 709 et al., 2014a) and the sum of the three output fluxes (pelagic, continental margin, redox-

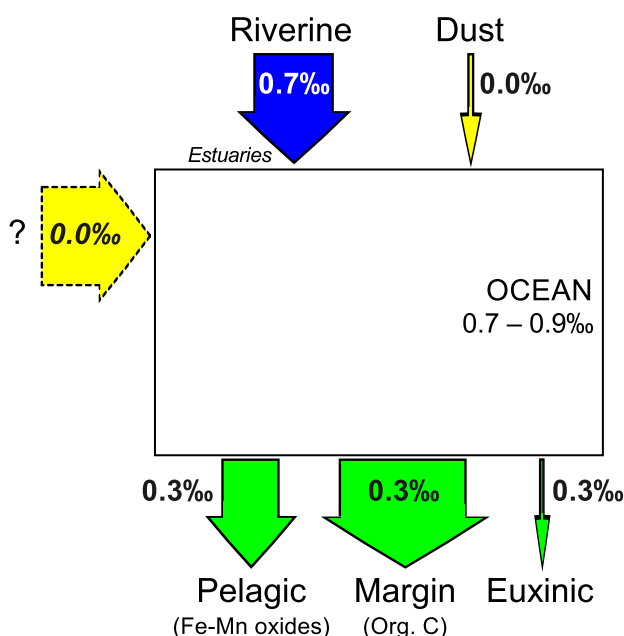
710 shuttle), we calculate a Cu oceanic residence time (where  $\tau$  = total inventory of element  $\div$   
 711 annual total input or output flux of element) of 2000 – 3200 years.

712

713 Together, the continental margin and pelagic Cu sinks sum to approximately twice the total  
 714 estimated riverine and dust input flux of Little et al. (2014a) ( $6.5 - 9.2 \times 10^8$  mol/yr). In  
 715 addition, all sedimentary sinks for Cu are isotopically light (at about +0.3‰) compared to  
 716 the isotope composition of the combined riverine and dust flux (at approximately +0.6‰,  
 717 Little et al., 2014a). If the Cu oceanic budget is at steady state, these observations require  
 718 either an additional sink that is isotopically heavy or (a) further source(s) that is/are  
 719 isotopically light. Given the flux imbalance (i.e., known output fluxes  $\gg$  known input  
 720 fluxes) and the fact that the major output fluxes have now been characterised, a missing  
 721 input flux appears more probable. Mass balance implies this missing source be  $\sim 9 \times 10^8$   
 722 mol/yr and have an isotope composition of  $\sim 0$ ‰, illustrated schematically in Figure 8.

723

724 **Figure 8.** Schematic illustrating the updated oceanic budget of Cu and Cu isotopes (after  
 725 Little et al., 2014a; 2015; this study). Arrows are scaled by flux magnitude and labelled  
 726 and coloured by isotope composition (yellow represents the isotopically light components,  
 727 blue the isotopically heavier components, and green is intermediate). The projected  
 728 missing source size and isotope composition is shown as a dashed arrow to the left of the  
 729 figure (see text for details). For reference to colours, please see online version of this  
 730 figure.



731

732

733 The main input of Cu to the modern ocean has typically been assumed to be the dissolved  
 734 phase in rivers (e.g., Little et al., 2014a). Two independent estimates put this riverine

735 dissolved flux at  $6 - 9 \times 10^8$  mol/yr (Gaillardet et al., 2003; Vance et al., 2008). This  
736 dissolved riverine flux is isotopically heavy, with a discharge-weighted riverine average  
737  $\delta^{65}\text{Cu}$  of +0.68‰ (Vance et al., 2008). These estimates assume conservative behaviour of  
738 Cu during estuarine mixing, as observed, for example, for two major river systems: the  
739 Chiang Jiang and the Amazon (Boyle et al., 1982; Edmond et al., 1985). However, non-  
740 conservative behaviour of Cu has also been observed in a spectrum of estuarine systems  
741 (e.g., Morris et al., 1978; Windom et al., 1983; Ackroyd et al., 1986). Furthermore, the  
742 dissolved flux of Cu accounts for only ~20% of the total riverine flux of Cu to the ocean,  
743 with the remainder delivered in particulate form (e.g., Martin and Meybeck, 1979). The  
744 partial dissolution of riverine particulates has recently been suggested as a significant  
745 oceanic source of several metals (e.g., Oelkers et al., 2012; Jones et al., 2012; 2014).  
746 Vance et al. (2008) report isotopically light Cu in the particulate phase of one small river  
747 system in the U.K, which is complementary to the heavy dissolved pool. Partial  
748 remobilisation of isotopically light riverine particulates, whether lithogenic or other (e.g.  
749 terrestrial organic matter) particles, may therefore provide one possible isotopically light  
750 flux of Cu to the ocean. Release could be envisaged in, e.g., anoxic estuarine  
751 environments, or further out in continental margin or open ocean settings. By analogy,  
752 release of neodymium (Nd) from the lithogenic phase has been hypothesised in continental  
753 margin settings (e.g., Jeandel et al., 2007; Pearce et al., 2013; Abbott et al., 2015; Abbott et  
754 al., 2016).

755

756 The natural (non-anthropogenic) dust flux of Cu to the ocean appears to be isotopically  
757 unfractionated from the lithogenic Cu source (at ~0‰), based on analysis of the water-  
758 leachable fraction of aerosols and loess particles (Little et al., 2014a; Dong et al., 2013).  
759 The magnitude of this natural dust flux has been calculated by two studies, one data-driven  
760 (Little et al., 2014a) and one model-based (Takano et al., 2014). In the data-driven  
761 approach, the flux is calculated based on a model of global dust deposition (Jickells et al.,  
762 2005), an estimate of the Cu concentration in UCC (35ppm; Rudnick and Gao, 2003), and  
763 an estimate of mineral dust solubility (27%; Desboeufs et al., 2005), yielding a Cu flux of  
764  $0.5 \times 10^8$  mol/yr (Little et al., 2014a). In the model-derived approach, Takano et al. (2014)  
765 invoked a much larger dust flux, at  $\sim 10 \times 10^8$  mol/yr, in order to balance their steady state  
766 model-derived output flux of  $17 \times 10^8$  mol/yr. The latter value is, itself, in line with the  
767 sum of the pelagic and continental margin sinks proposed here. Assuming a lithogenic  
768 isotope composition (0‰) for their postulated dust flux, Takano et al. (2014) further

769 calculate that the Cu isotope composition of the output flux should be +0.3‰ (Takano et  
770 al., 2014), also consistent with results in this study. Nevertheless, we consider a very large  
771 dust flux to be rather unlikely, due in part to the low solubility of Cu in dust (e.g.,  
772 Desboeufs et al., 2005; Sholkovitz et al., 2010). Even if mineral dust were completely  
773 soluble – for example, if solubility is enhanced by the presence of organic ligands (as  
774 suggested for Fe; Fishwick et al., 2014) – the maximum Cu input flux possible based on an  
775 estimate of global mineral dust deposition and the Cu concentration in UCC is five times  
776 lower than that required by Takano et al. (2014), at  $2.0 \times 10^8$  mol/yr.

777

778 Of other possible inputs, a hydrothermal Cu source has to date been assumed to be globally  
779 insignificant due its to efficient removal close to the vent (e.g., Trocine and Trefry, 1988;  
780 German et al., 1991; 2002). Scavenging within the Atlantic TAG hydrothermal plume  
781 indicates that hydrothermal activity may in fact be a net sink of Cu, at least in certain  
782 environments (Jacquot and Moffett, 2015; Roshan and Wu, 2015). However, recent water  
783 column data for a range of trace elements and their isotopes, collected as part of the  
784 international GEOTRACES program, has highlighted significant basin scale heterogeneity  
785 in the iron (Fe) and zinc (Zn) hydrothermal flux, indicating that this potential source  
786 should be re-evaluated (Resing et al., 2015; Roshan et al., 2016). Sander and Koschinsky  
787 (2011) suggest that organic complexation may be one means to stabilise metals from  
788 hydrothermal vent sources in the dissolved phase. Primary hydrothermal fluxes are likely  
789 to have a lithogenic Cu isotope composition (at ~0‰), though these may be subject to  
790 considerable secondary isotope fractionation effects resulting from sulphide precipitation,  
791 organic complexation, and/or scavenging to oxide phases.

792

793 Benthic fluxes have long been considered to play a role in the water column distribution of  
794 dissolved Cu (e.g., Boyle et al., 1977). In terms of oceanic mass balance, there are two  
795 ways in which such a benthic flux can be envisaged, which differ according to the solid  
796 phase from which the Cu is released to bottom waters. The first requires that Cu be  
797 released from external sources, either via rivers (as discussed above), or hydrothermal  
798 particulates. This possibility would then represent a true new source of Cu to the ocean and  
799 might be expected to be isotopically light if lithogenic or hydrothermal material is the  
800 source. The second type of benthic flux involves re-release to bottom waters of  
801 bioauthigenic Cu (i.e., Cu from the water column). This process may occur in porewaters  
802 of suboxic sediments, where suboxic denotes negligible dissolved oxygen and sulphide.

803 Under these conditions, Cu carrier phases (Fe-Mn oxides, organic matter) are reduced, and  
804 Cu could diffuse into bottom water (Shaw et al., 1990; Elderfield et al., 1981; Heggie et al.,  
805 1987; Klinkhammer, 1980; Sawlan and Murray, 1983). This process may be aided by  
806 complexation to strong organic ligands in porewaters (Skrabal et al., 1997; 2000; Shank et  
807 al., 2004a; 2004b). In itself, this process does not constitute a true new source of Cu to the  
808 oceans, because the Cu that is returned to the water column came from the water column –  
809 i.e., the Cu is recycled. Note that any such recycling is implicit in the calculation of the  
810 organic C burial-associated Cu flux (i.e., this is a net flux). This recycling could, however,  
811 be accompanied by an isotopic effect, if isotope fractionation occurs in the sediment pile.  
812 An isotopically light signature for such a source would require preferential retention of  
813 heavy Cu isotopes in the solid phase. This direction of fractionation would not be  
814 consistent, however, with what would be predicted based on organic complexation of Cu in  
815 pore waters. This process is likely to favour retention of heavy Cu isotopes in the soluble  
816 phase, with the removal of light Cu isotopes to particles.

817

818 Ultimately, we suggest that better resolution of the Cu isotope budget requires future  
819 studies focussing on: (1) an improved evaluation of the diagenetic processing of Cu and its  
820 isotopes, (2) the fate and isotopic signature of hydrothermally sourced Cu, and (3) the  
821 behaviour of continent-derived particulate Cu in the marine environment, both in estuaries  
822 and more distally.

823

824

## 825 **6. Conclusions and Outlook**

826

827 This study presents a Cu isotope dataset for recent organic rich sediments from a range of  
828 low oxygen and reducing sedimentary environments. The data indicate that the modern  
829 bioauthigenic (i.e., non-lithogenic) oceanic Cu output flux is isotopically homogeneous  
830 across many sedimentary environments – at about +0.3‰. This value is significantly  
831 lighter than the isotope composition of the open oceans, at +0.6 to +0.9‰. We suggest that  
832 the homogeneous isotopic composition of the Cu output flux reflects either (1) an  
833 equilibrium isotope fractionation between two species in the dissolved phase, with an  
834 isotopically heavy dissolved pool complexed by strong organic ligands and a particle  
835 reactive, isotopically light free Cu<sup>2+</sup> pool, or (2) an equilibrium isotope fractionation  
836 directly between the organically complexed dissolved pool and the particulate phase. In the

837 latter scenario all particulates would be required to exhibit the same fractionation from the  
838 dissolved pool. In either case, continuous reversible exchange between sinking particulates  
839 and the dissolved pool, all the way down through the water column, may contribute to the  
840 homogeneity of the output flux.

841

842 Unexpectedly, highly Cu enriched euxinic Black Sea sediments (with  $\delta^{65}\text{Cu}_{\text{auth}}$  of +0.3‰)  
843 do not record the Cu isotope signature of the open ocean (at around +0.6 to +0.9‰),  
844 despite near quantitative removal of Cu from the water column. We hypothesize that this  
845 signature reflects active Fe-Mn cycling at the Black Sea redoxcline, with shuttling of  
846 isotopically 'bioauthigenic' Cu (i.e., at +0.3‰) to the restricted deep basin where it is  
847 removed to sediment via sulphide precipitation. A similar process, albeit on a smaller  
848 length-scale, likely also occurs at the sediment-water interface of suboxic to anoxic  
849 continental margin sediments (e.g., San Nicolas Basin) and is also evident in the modern-  
850 day near-chemocline station of the Black Sea (Station 16B). In all cases, we envisage that  
851 an isotopically heavy pool of Cu is retained in the dissolved phase via complexation to  
852 strong organic ligands.

853

854 Low oxygen conditions alone are not sufficient to generate strong enrichment of Cu in  
855 marine sediments. Variability in the dataset presented here can be explained to first order  
856 in terms of dilution of the bioauthigenic signature (at about +0.3‰) with lithogenic  
857 material (at ~0‰), and the lithogenic sedimentary accumulation rate is a strong control on  
858 the presence or absence of the bioauthigenic  $\delta^{65}\text{Cu}$  signature in sediments.

859

860 We note that all characterised sinks for Cu in the modern ocean are isotopically light (at  
861 about +0.3‰) relative to the current best estimate for the input flux (at about +0.6‰; Little  
862 et al., 2014a). This disparity indicates the presence of an as yet unidentified isotopically  
863 light source, of approximately lithogenic composition (~0‰; Fig. 8). Dust is one such  
864 possible light source, as previously suggested by Takano et al. (2014). We suggest two  
865 other possible light sources of Cu: (1) hydrothermal input, (2) partial dissolution of  
866 continentally derived particulates. Distinguishing among these three possible input fluxes  
867 requires future detailed research.

868

869 Finally, our findings, along with those of several previous studies, indicate that strong  
870 organic ligands play a key role in the modern biogeochemical cycle of Cu and Cu isotopes.

871 This role must be fully considered in future studies seeking to apply Cu isotopes in the  
872 rock record as a paleoceanographic tracer.

873

874

## 875 **Acknowledgments**

876

877 The authors would like to thank three anonymous reviewers and the associate editor R.  
878 James for comments that significantly improved the manuscript. Little is supported by a  
879 Leverhulme early career fellowship at Imperial. Isotopic measurements at Bristol were  
880 supported by a NERC-funded PhD studentship NE/H525111/1 to Little. The ETH Zürich  
881 project work was supported by Swiss National Science Foundation Project 200021\_153087  
882 to Vance. Continental margin sediment sample collection was supported by multiple US  
883 NSF grants to McManus including OCE-0624777 and OCE-0219651. McManus was also  
884 supported by U.S. National Science Foundation grant OCE-1657832. Lyons is grateful for  
885 support from the NASA Astrobiology Institute and the NSF FESD and ELT programs. We  
886 thank William Berelson and Gary Klinkhammer for their contributions to cruises where  
887 some of these samples were collected, and Chris Coath and Corey Archer for facilitating  
888 the smooth running of clean labs and mass spectrometers in Bristol and Zürich.

889

890

891

## 892 **References**

893 Abbott, A. N., Haley, B. A., and McManus, J. (2015). Bottoms up: Sedimentary control of  
894 the deep North Pacific Ocean's  $\epsilon\text{Nd}$  signature. *Geology* **43**(11), 1035–1035.

895 Abbott, A. N., Haley, B. A., and McManus, J. (2016). The impact of sedimentary coatings  
896 on the diagenetic Nd flux. *Earth Planet. Sci. Lett.* **449**, 217–227.

897 Ackroyd, D. R., Bale, A. J., Howland, R. J. M., Knox, S., Millward, G. E., and Morris, A.  
898 W. (1986). Distributions and behaviour of dissolved Cu, Zn and Mn in the Tamar  
899 Estuary. *Estuar. Coast. Shelf S.* **23**(5), 621–640.

900 Albarède, F. (2004) The stable isotope geochemistry of copper and zinc. *Rev. Mineral.*  
901 *Geochem.* **55**(1), 409–427.

902 Algeo, T., and Lyons, T. (2006) Mo–total organic carbon covariation in modern anoxic  
903 marine environments: Implications for analysis of paleoredox and paleohydrographic  
904 conditions. *Paleoceanography* **21**(1), PA1016.

905 Algeo, T. J., and Maynard, J. B. (2004) Trace-element behavior and redox facies in core  
906 shales of Upper Pennsylvanian Kansas-type cyclothems. *Chem. Geol.* **206**(3–4), 289–  
907 318.

- 908 Archer C. and Vance D. (2004) Mass discrimination correction in multiple-collector  
909 plasma source mass spectrometry: an example using Cu and Zn isotopes. *J. Anal. At.*  
910 *Spectrom.* **19**(5), 656–665.
- 911 Arnold, G. L., Anbar, A. D., Barling, J., and Lyons, T. W. (2004) Molybdenum isotope  
912 evidence for widespread anoxia in mid-Proterozoic oceans. *Science* **304**(5667), 87–90.
- 913 Asael, D., Matthews, A., Bar-Matthews, M., and Halicz, L. (2007). Copper isotope  
914 fractionation in sedimentary copper mineralization (Timna Valley, Israel). *Chem.*  
915 *Geol.* **243**(3), 238–254.
- 916 Barling, J., and Anbar, A. D. (2004). Molybdenum isotope fractionation during adsorption  
917 by manganese oxides. *Earth Planet. Sci. Lett.* **217**(3), 315–329.
- 918 Barling, J., Arnold, G. L., and Anbar, A. D. (2001). Natural mass-dependent variations in  
919 the isotopic composition of molybdenum. *Earth Planet. Sci. Lett.* **193**(3), 447–457.
- 920 Berelson, W. M. (1991). The flushing of two deep-sea basins, southern California  
921 borderland. *Limnol. Oceanogr.* **36**(6), 1150–1166.
- 922 Berelson, W. M., Hammond, D. E., and Johnson, K. S. (1987). Benthic fluxes and the  
923 cycling of biogenic silica and carbon in two southern California borderland basins.  
924 *Geochim. Cosmochim. Acta* **51**(6), 1345–1363.
- 925 Berelson, W. M., McManus, J., Coale, K. H., Johnson, K. S., Kilgore, T., Burdige, D., and  
926 Pilskaln, C. (1996). Biogenic matter diagenesis on the sea floor: A comparison  
927 between two continental margin transects. *J. Mar Res.* **54**(4), 731–762.
- 928 Berelson, W. M., Prokopenko, M., Sansone, F. J., Graham, A. W., McManus, J., and  
929 Bernhard, J. M. (2005). Anaerobic diagenesis of silica and carbon in continental  
930 margin sediments: discrete zones of TCO<sub>2</sub> production. *Geochim. Cosmochim. Acta*  
931 **69**(19), 4611–4629.
- 932 Bermin J., Vance D., Archer C. and Statham P. J. (2006) The determination of the isotopic  
933 composition of Cu and Zn in seawater. *Chem. Geol.* **226**(3–4), 280–297.
- 934 Bigalke, M., Weyer, S., and Wilcke, W. (2010). Copper isotope fractionation during  
935 complexation with insolubilized humic acid. *Environ. Sci. Technol.* **44**(14), 5496–  
936 5502.
- 937 Böning, P., Brumsack, H., Böttcher, M. E., Schnetger, B., Kriete, C., Kallmeyer, J., and  
938 Borchers, S. L. (2004) Geochemistry of Peruvian near-surface sediments. *Geochim.*  
939 *Cosmochim. Acta* **68**(21), 4429–4451.
- 940 Böning, P., Cuypers, S., Grunwald, M., Schnetger, B., and Brumsack, H. J. (2005).  
941 Geochemical characteristics of Chilean upwelling sediments at ~ 36 S. *Mar. Geol.*  
942 **220**(1), 1–21.
- 943 Böning, P., Fröllje, H., Beck, M., Schnetger, B., and Brumsack, H. J. (2012).  
944 Underestimation of the authigenic fraction of Cu and Ni in organic-rich sediments.  
945 *Mar. Geol.* **323**, 24–28.
- 946 Boyle, E. A., Sclater, F. R., and Edmond, J. M. (1977). The distribution of dissolved  
947 copper in the Pacific. *Earth Planet. Sci. Lett.* **37**(1), 38–54.
- 948 Bruland, K. W. (1980). Oceanographic distributions of cadmium, zinc, nickel, and copper  
949 in the North Pacific. *Earth Planet. Sci. Lett.* **47**(2), 176–198.

- 950 Bruland K. W. and Lohan M. C. (2003) Controls of Trace Metals in Seawater. Pergamon,  
951 Oxford, 23–47.
- 952 Bruland K. W., Orians K. J. and Cowen J. P. (1994) Reactive trace metals in the stratified  
953 central North Pacific. *Geochim. Cosmochim. Acta* **58**(15), 3171–3182.
- 954 Bruland, K. W., Koide, M., and Goldberg, E. D. (1974). The comparative marine  
955 geochemistries of lead 210 and radium 226. *J. Geophys. Res.* **79**(21), 3083–3086.
- 956 Bruland, K. W., Franks, R. P., Landing, W. M., and Soutar, A. (1981). Southern California  
957 inner basin sediment trap calibration. *Earth Planet. Sci. Lett.* **53**(3), 400–408.
- 958 Brumsack H. (2006) The trace metal content of recent organic carbon-rich sediments:  
959 implications for cretaceous black shale formation. *Palaeogeogr. Palaeoclimatol.*  
960 *Palaeoecol.* **232**(2), 344–361.
- 961 Buesseler, K. O., and Benitez, C. R. (1994). Determination of mass accumulation rates and  
962 sediment radionuclide inventories in the deep Black Sea. *Deep Sea Res. Pt I* **41**(11),  
963 1605–1615.
- 964 Calvert S. and Pedersen T. (1993) Geochemistry of recent oxic and anoxic marine  
965 sediments: implications for the geological record. *Mar. Geol.* **113**(1), 67–88.
- 966 Canfield, D. E. (1998). A new model for Proterozoic ocean chemistry. *Nature* **396**(6710),  
967 450–453.
- 968 Chong, L. S., Prokopenko, M. G., Berelson, W. M., Townsend-Small, A., and McManus, J.  
969 (2012). Nitrogen cycling within suboxic and anoxic sediments from the continental  
970 margin of Western North America. *Mar. Chem.* **128**, 13–25.
- 971 Coale K. H. and Bruland K. W. (1988) Copper complexation in the Northeast Pacific.  
972 *Limnol. Oceanogr.* **33**(5), 1084–1101.
- 973 Coale, K. H., and Bruland, K. W. (1990). Spatial and temporal variability in copper  
974 complexation in the North Pacific. *Deep Sea Res.* **37**(2), 317–336.
- 975 Conway, T. M., and John, S. G. (2014). Quantification of dissolved iron sources to the  
976 North Atlantic Ocean. *Nature* **511**(7508), 212–215.
- 977 Dean, W. E., Piper, D. Z., and Peterson, L. C. (1999) Molybdenum accumulation in  
978 Cariaco Basin sediment over the past 24 k.y.: A record of water-column anoxia and  
979 climate. *Geology* **27**(6), 507–510.
- 980 Desboeufs K., Sofikitis A., Losno R., Colin J. and Ausset P. (2005) Dissolution and  
981 solubility of trace metals from natural and anthropogenic aerosol particulate matter.  
982 *Chemosphere* **58**(2), 195–203.
- 983 Deutsch, C., Berelson, W., Thunell, R., Weber, T., Tams, C., McManus, J., Crusius, J., Ito,  
984 T., Baumgartner, T., Ferreira, V., Mey, J., and van Geen, A. (2014). Centennial  
985 changes in North Pacific anoxia linked to tropical trade winds. *Science* **345**(6197),  
986 665–668.
- 987 Dong, S., Weiss, D. J., Strekopytov, S., Kreissig, K., Sun, Y., Baker, A. R., and Formenti,  
988 P. (2013). Stable isotope ratio measurements of Cu and Zn in mineral dust (bulk and  
989 size fractions) from the Taklimakan Desert and the Sahel and in aerosols from the  
990 eastern tropical North Atlantic Ocean. *Talanta* **114**, 103–109.
- 991 Douville, E., Charlou, J.-L., Oelkers, E.H., Bienvenu, P., Jove Colan, C.F., Donval, J.P.,  
992 Fouquet, Y., Prieur, D. and Appriou, P. (2002). The Rainbow vent fluids (36°14'N,

- 993 MAR): the influence of ultramafic rocks and phase separation on trace metal content  
994 in Mid-Atlantic Ridge hydrothermal fluids. *Chem. Geol.* **184**, 37–48.
- 995 Dryden, C. L., Gordon, A. S., and Donat, J. R. (2004). Interactive regulation of dissolved  
996 copper toxicity by an estuarine microbial community. *Limnol. Oceanogr.* **49**(4), 1115–  
997 1122.
- 998 Ehrlich, S., Butler, I., Halicz, L., Rickard, D., Oldroyd, A., and Matthews, A. (2004).  
999 Experimental study of the copper isotope fractionation between aqueous Cu (II) and  
1000 covellite, CuS. *Chemical Geology* **209**(3), 259–269.
- 1001 Elderfield, H. (1981). Metal-organic associations in interstitial waters of Narragansett Bay  
1002 sediments. *Am. J. Sci.* **281**(9), 1184–1196.
- 1003 Elderfield, H., Luedtke, N., McCaffrey, R. J., and Bender, M. (1981) Benthic flux studies  
1004 in Narragansett Bay. *Am. J. Sci.* **281**(6), 768–787.
- 1005 Elrod, V. A., Johnson, K. S., and Coale, K. H. (1991). Determination of subnanomolar  
1006 levels of iron (II) and total dissolved iron in seawater by flow injection and analysis  
1007 with chemiluminescence detection. *Anal. Chem.* **63**(9), 893–898.
- 1008 Emerson, S. R., and Husted, S. S. (1991). Ocean anoxia and the concentrations of  
1009 molybdenum and vanadium in seawater. *Mar. Chem.* **34**(3–4), 177–196.
- 1010 Emery, K. O. (1954). General geology of the offshore area, southern California. *Bull.*  
1011 *Calif. Div. Mines Geol.* **170**, 107–111.
- 1012 Emery, K. O. (1960). Basin plains and aprons off southern California. *J. Geology*, 464–  
1013 479.
- 1014 Emeis, K. C., Whelan, J. K., and Tarafa, M. (1991) Sedimentary and geochemical  
1015 expressions of oxic and anoxic conditions on the Peru shelf. Geological Society,  
1016 London, Special Publications **58**(1), 155–170.
- 1017 Eppley, R. W. (1992). Chlorophyll, photosynthesis and new production in the Southern  
1018 California Bight. *Prog. Oceanogr.* **30**(1-4), 117–150.
- 1019 Finney, B., and Huh, C. A. (1989). High resolution sedimentary records of heavy metals  
1020 from the Santa Monica and San Pedro Basins, California. *Marine Poll. Bull.* **20**(4),  
1021 181–187.
- 1022 Fishwick, M. P., P. N. Sedwick, M. C. Lohan, P. J. Worsfold, K. N. Buck, T. M. Church,  
1023 and S. J. Ussher (2014), The impact of changing surface ocean conditions on the  
1024 dissolution of aerosol iron, *Global Biogeochem. Cycles* **28**, 1235–1250.
- 1025 Francois R. (1988) A study on the regulation of the concentrations of some trace metals  
1026 (Rb, Sr, Zn, Pb, Cu, V, Cr, Ni, Mn and Mo) in Saanich Inlet Sediments, British  
1027 Columbia, Canada. *Mar. Geol.* **83**(1), 285–308.
- 1028 Fujii, T., Moynier, F., Abe, M., Nemoto, K., and Albarède, F. (2013). Copper isotope  
1029 fractionation between aqueous compounds relevant to low temperature geochemistry  
1030 and biology. *Geochim. Cosmochim. Acta* **110**, 29–44.
- 1031 Gaillardet J., Viers J. and Dupré B. (2003) Trace elements in river waters. *Treatise*  
1032 *Geochem.* **5**, 225–272.
- 1033 German C. R., Campbell A. C. and Edmond J. M. (1991) Hydrothermal scavenging at the  
1034 mid-Atlantic ridge: modification of trace element dissolved fluxes. *Earth Planet. Sci.*  
1035 *Lett.* **107**(1), 101–114.

- 1036 German C. R., Colley S., Palmer M. R., Khripounoff A. and Klinkhammer G. P. (2002)  
 1037 Hydrothermal plume-particle fluxes at 13 N on the East Pacific Rise. *Deep Sea Res.*  
 1038 **49**(11), 1921–1940.
- 1039 Goni, M. A., Aceves, H. L., Thunell, R. C., Tappa, E., Black, D., Astor, Y., ... and Muller-  
 1040 Karger, F. (2003). Biogenic fluxes in the Cariaco Basin: a combined study of sinking  
 1041 particulates and underlying sediments. *Deep Sea Res. Pt I.* **50**(6), 781–807.
- 1042 Gordon, A. S., Dyer, B. J., Kango, R. A., and Donat, J. R. (1996). Copper ligands isolated  
 1043 from estuarine water by immobilized metal affinity chromatography: temporal  
 1044 variability and partial characterization. *Mar. Chem.* **53**(3), 163–172.
- 1045 Haraldsson, C., and Westerlund, S. (1991). Total and suspended cadmium, cobalt, copper,  
 1046 iron, lead, manganese, nickel, and zinc in the water column of the Black Sea. In *Black*  
 1047 *Sea Oceanography* (pp. 161–172). Springer Netherlands.
- 1048 Hartnett, H. E., Keil, R. G., Hedges, J. I., and Devol, A. H. (1998). Influence of oxygen  
 1049 exposure time on organic carbon preservation in continental margin sediments. *Nature*  
 1050 **391**(6667), 572–575.
- 1051 Haug, G. H., Pedesen, T. F., Sigman, D. M., Calvert, S. E., Nielsen, B., and Peterson, L. C.  
 1052 (1998) Glacial/interglacial variations in production and nitrogen fixation in the  
 1053 Cariaco Basin during the last 580 kyr. *Paleoceanography* **13**(5), 427–432.
- 1054 Heggie, D., Klinkhammer, G., and Cullen, D. (1987). Manganese and copper fluxes from  
 1055 continental margin sediments. *Geochim. Cosmochim. Acta* **51**(5), 1059–1070.
- 1056 Huh, C. A., Small, L. F., Niemi, S., Finney, B. P., Hickey, B. M., Kachel, N. B., ... and  
 1057 Williams, P. M. (1990). Sedimentation dynamics in the Santa Monica-San Pedro  
 1058 Basin off Los Angeles: radiochemical, sediment trap and transmissometer studies.  
 1059 *Cont. Shelf Res.* **10**(2), 137–164.
- 1060 Jacobs L., Emerson S. and Huested S. (1987) Trace metal geochemistry in the Cariaco  
 1061 Trench. *Deep Sea Res.* **34**(5), 965–981.
- 1062 Jacobs L., Emerson S. and Skei J. (1985) Partitioning and transport of metals across the O<sub>2</sub>  
 1063 H<sub>2</sub>S interface in a permanently anoxic basin: Framvaren Fjord, Norway. *Geochim.*  
 1064 *Cosmochim. Acta* **49**(6), 1433–1444.
- 1065 Jacquot, J. E., and Moffett, J. W. (2015). Copper distribution and speciation across the  
 1066 International GEOTRACES Section GA03. *Deep Sea Res. Pt II* **116**, 187–207.
- 1067 Jeandel, C., Arsouze, T., Lacan, F., Techine, P., and Dutay, J. C. (2007). Isotopic Nd  
 1068 compositions and concentrations of the lithogenic inputs into the ocean: A  
 1069 compilation, with an emphasis on the margins. *Chem. Geol.* **239**(1), 156–164.
- 1070 Jickells T., An Z., Andersen K. K., Baker A., Bergametti G., Brooks N., Cao J., Boyd P.,  
 1071 Duce R. and Hunter K., et al. (2005) Global iron connections between desert dust,  
 1072 ocean biogeochemistry, and climate. *Science* **308**(5718), 67–71.
- 1073 Johnson, K., Purvis, G., Lopez-Capel, E., Peacock, C., Gray, N., Wagner, T., ... and  
 1074 Robertson, S. (2015). Towards a mechanistic understanding of carbon stabilization in  
 1075 manganese oxides. *Nat. Commun.* **6**, 7628.
- 1076 Jones, M. T., Pearce, C. R., Jeandel, C., Gislason, S. R., Eiriksdottir, E. S., Mavromatis,  
 1077 V., and Oelkers, E. H. (2012). Riverine particulate material dissolution as a significant  
 1078 flux of strontium to the oceans. *Earth Planet. Sci. Lett.* **355**, 51–59.

- 1079 Jones, M. T., Gislason, S. R., Burton, K. W., Pearce, C. R., Mavromatis, V., von  
1080 Strandmann, P. A. P., and Oelkers, E. H. (2014). Quantifying the impact of riverine  
1081 particulate dissolution in seawater on ocean chemistry. *Earth Planet. Sci. Lett.* **395**,  
1082 91–100.
- 1083 Keeling, R. F., Körtzinger, A., and Gruber, N. (2010). Ocean deoxygenation in a warming  
1084 world. *Marine Science* **2**.
- 1085 Klinkhammer, G. P. (1980). Early diagenesis in sediments from the eastern equatorial  
1086 Pacific, II. Pore water metal results. *Earth Planet. Sci. Lett.* **49**(1), 81–101.
- 1087 Kuwabara, J. S., Topping, B. R., Coale, K. H., and Berelson, W. M. (1999). Processes  
1088 affecting the benthic flux of trace metals into the water column of San Francisco Bay.  
1089 In *US Geological Survey Toxic Substances Hydrology Program--Proceedings of the*  
1090 *Technical Meeting, Charleston, South Carolina* **2**, 115–119.
- 1091 Laglera, L. M., and van den Berg, C. M. (2003). Copper complexation by thiol compounds  
1092 in estuarine waters. *Mar. Chem.* **82**(1), 71–89.
- 1093 Lalonde, K., Mucci, A., Ouellet, A., and Gélinas, Y. (2012). Preservation of organic matter  
1094 in sediments promoted by iron. *Nature* **483**(7388), 198–200.
- 1095 Leal, M. F. C., and Van Den Berg, C. M. (1998). Evidence for strong copper (I)  
1096 complexation by organic ligands in seawater. *Aquat. Geochem.* **4**(1), 49–75.
- 1097 Li, C., Love, G. D., Lyons, T. W., Fike, D. A., Sessions, A. L., and Chu, X. (2010a). A  
1098 stratified redox model for the Ediacaran ocean. *Science* **328**(5974), 80–83.
- 1099 Li, X., Gilhooly, W. P., III, Zerkle, A. L., Lyons, T. W., Farquhar, J., Werne, J. P., Varela,  
1100 R., and Scranton, M. L. (2010b) Stable sulfur isotopes in the water column of the  
1101 Cariaco Basin. *Geochim. Cosmochim. Acta* **74**(23), 6764–6778.
- 1102 Li, X., Cutter, G. A., Thunell, R. C., Tappa, E., Gilhooly, W. P., III, Lyons, T. W., Astor,  
1103 Y., and Scranton, M. I. (2011) Particulate sulfur species in the water column of the  
1104 Cariaco Basin. *Geochim. Cosmochim. Acta* **75**(1), 148–163.
- 1105 Little, S. H., Vance, D., Walker-Brown, C., and Landing, W. M. (2014a) The oceanic mass  
1106 balance of copper and zinc isotopes, investigated by analysis of their inputs, and  
1107 outputs to ferromanganese oxide sediments. *Geochim. Cosmochim. Acta* **125**, 673–  
1108 693.
- 1109 Little, S. H., Sherman, D. M., Vance, D., and Hein, J. R. (2014b). Molecular controls on  
1110 Cu and Zn isotopic fractionation in Fe–Mn crusts. *Earth Planet. Sci. Lett.* **396**, 213–  
1111 222.
- 1112 Little, S. H., Vance, D., Lyons, T. W., and McManus, J. (2015). Controls on trace metal  
1113 authigenic enrichment in reducing sediments: Insights from modern oxygen-deficient  
1114 settings. *Am. J. Sci.* **315**(2), 77–119.
- 1115 Little, S. H., Vance, D., McManus, J., and Severmann, S. (2016). Key role of continental  
1116 margin sediments in the oceanic mass balance of Zn and Zn isotopes. *Geology* **44**(3),  
1117 207–210.
- 1118 Lucia, M., Campos, A. M., and van den Berg, C. M. (1994). Determination of copper  
1119 complexation in sea water by cathodic stripping voltammetry and ligand competition  
1120 with salicylaldoxime. *Anal. Chim. Acta* **284**(3), 481–496.

- 1121 Lückge, A., and Reinhardt, L. (2000) CTD measurements in the water column off Peru, in  
 1122 Kudrass, H. R., editor, Cruise report SO147 Peru Upwelling: Valparaiso-Callao,  
 1123 29.05-03.07, 35–37.
- 1124 Lyons, T. W. (1991) Upper Holocene sediments of the Black Sea: Summary of Leg 4 box  
 1125 cores (1988 Black Sea oceanographic expedition), in Izdar, E., and Murray, J. W.,  
 1126 editors, Black Sea Oceanography. NATO ASI Series **351**, 401–441.
- 1127 Lyons, T. W. (1997) Sulfur isotopic trends and pathways of iron sulfide formation in upper  
 1128 Holocene sediments of the anoxic Black Sea. *Geochim. Cosmochim. Acta* **61**(16),  
 1129 3367–3382.
- 1130 Lyons, T. W., and Berner, R. A. (1992) Carbon-sulfur-iron systematics of the uppermost  
 1131 deep-water sediments of the Black Sea. *Chem. Geol.* **99**(1–3), 1–27.
- 1132 Lyons, T. W., and Severmann, S. (2006) A critical look at iron paleoredox proxies: New  
 1133 insights from modern euxinic marine basins. *Geochim. Cosmochim. Acta* **70**(23),  
 1134 5698–5722.
- 1135 Lyons, T. W., Berner, R. A., and Anderson, R. F. (1993) Evidence for large pre-industrial  
 1136 perturbations of the Black Sea chemocline. *Nature* **365**, p. 538–540,
- 1137 Lyons, T. W., Werne, J. P., Hollander, D. J., and Murray, R. W. (2003) Contrasting sulfur  
 1138 geochemistry and Fe/Al and Mo/Al ratios across the last oxic-to-anoxic transition in  
 1139 the Cariaco Basin, Venezuela. *Chem. Geol.* **195**(1–4), 131–157.
- 1140 Lyons, T. W., Reinhard, C., and Planavsky, N. (2014) The rise of oxygen in Earth’s early  
 1141 ocean and atmosphere. *Nature* **506**, 307–315.
- 1142 Macías, D., Franks, P. J., Ohman, M. D., and Landry, M. R. (2012). Modeling the effects  
 1143 of coastal wind-and wind–stress curl-driven upwellings on plankton dynamics in the  
 1144 Southern California current system. *J. Marine Sys.* **94**, 107–119.
- 1145 Malouta, D. N., Gorsline, D. S., and Thornton, S. E. (1981). Processes and rates of recent  
 1146 (Holocene) basin filling in an active transform margin: Santa Monica Basin, California  
 1147 Continental Borderland. *J. Sed. Res.* **51**(4).
- 1148 Maréchal C. N., Telouk P. and Albarède F. (1999) Precise analysis of copper and zinc  
 1149 isotopic compositions by plasma-source mass spectrometry. *Chem. Geol.* **156**(1–4),  
 1150 251–273.
- 1151 Martinez, N. C., Murray, R. W., Thunell, R. C., Peterson, L. C., Muller-Karger, F.,  
 1152 Lorenzoni, L., ... and Varela, R. (2010). Local and regional geochemical signatures of  
 1153 surface sediments from the Cariaco Basin and Orinoco Delta, Venezuela. *Geology*  
 1154 **38**(2), 159–162.
- 1155 Mathur, R., Titley, S., Barra, F., Brantley, S., Wilson, M., Phillips, A., ... and Hart, G.  
 1156 (2009). Exploration potential of Cu isotope fractionation in porphyry copper  
 1157 deposits. *J. Geochem. Explor.* **102**(1), 1–6.
- 1158 Martin, J. M., and Meybeck, M. (1979). Elemental mass-balance of material carried by  
 1159 major world rivers. *Mar. Chem.* **7**(3), 173–206.
- 1160 McManus, J., Berelson, W. M., Coale, K. H., Johnson, K. S., and Kilgore, T. E. (1997).  
 1161 Phosphorus regeneration in continental margin sediments. *Geochim. Cosmochim. Acta*  
 1162 **61**(14), 2891–2907.
- 1163 McManus, J., Berelson, W. M., Klinkhammer, G. P., Johnson, K. S., Coale, K. H.,  
 1164 Anderson, R. F., ... and McCorkle, D. C. (1998). Geochemistry of barium in marine

- 1165 sediments: Implications for its use as a paleoproxy. *Geochim. Cosmochim. Acta*  
 1166 **62**(21), 3453–3473.
- 1167 McManus J., Berelson W., Severmann S., Poulson R., Hammond D., Klinkhammer G. and  
 1168 Holm C. (2006) Molybdenum and uranium geochemistry in continental margin  
 1169 sediments: paleoproxy potential. *Geochim. Cosmochim. Acta* **70**(18), 4643–4662.
- 1170 Moffett J. W. and Brand L. E. (1996) Production of strong, extracellular Cu chelators by  
 1171 marine cyanobacteria in response to Cu stress. *Limnol. Oceanogr.* **41**(3), 388–395.
- 1172 Moffett J. W. and Dupont C. (2007) Cu complexation by organic ligands in the sub-arctic  
 1173 NW Pacific and Bering Sea. *Deep Sea Res. Pt I* **54**(4), 586–595.
- 1174 Moffett, J. W., Zika, R. G., and Brand, L. E. (1990). Distribution and potential sources and  
 1175 sinks of copper chelators in the Sargasso Sea. *Deep Sea Res.* **37**(1), 27–36.
- 1176 Morford, J. L., and Emerson, S. (1999). The geochemistry of redox sensitive trace metals  
 1177 in sediments. *Geochim. Cosmochim. Acta* **63**(11), 1735–1750.
- 1178 Morris, A. W., Mantoura, R. F. C., Bale, A. J., and Howland, R. J. M. (1978). Very low  
 1179 salinity regions of estuaries: important sites for chemical and biological  
 1180 reactions. *Nature* **274**(5672), 678–680.
- 1181 Moynier, F., Vance, D., Fujii, T., Savage, P. (in press) The Isotope Geochemistry of Zinc  
 1182 and Copper. *Rev. Mineral. Geochem.* **82**.
- 1183 Muller, F. L. L., Gulin, S. B., and Kalvøy, A. (2001) Chemical speciation of copper and  
 1184 zinc in surface waters of the western Black Sea. *Mar. Chem.* **76**(4), 233–251.
- 1185 Muñoz, P., Lange, C. B., Gutiérrez, D., Hebbeln, D., Salamanca, M. A., Dezileau, L., ...  
 1186 and Benninger, L. K. (2004). Recent sedimentation and mass accumulation rates based  
 1187 on <sup>210</sup>Pb along the Peru–Chile continental margin. *Deep Sea Res. Pt II* **51**(20), 2523–  
 1188 2541.
- 1189 Murray, J. W., Jannasch, H. W., Honjo, S., Anderson, R. F., Reeburgh, W. S., Top, Z.,  
 1190 Friederich, G. E., Codispoti, L. A., and Izdar, E. (1989) Unexpected changes in the  
 1191 oxic/anoxic interface in the Black Sea. *Nature* **338**, 411–413
- 1192 Murray, J. W., Top, Z., and Özsoy, E. (1991). Hydrographic properties and ventilation of  
 1193 the Black Sea. *Deep Sea Res.* **38**, S663-S689.
- 1194 Nägler T., Neubert N., Böttcher M., Dellwig O. and Schnetger B. (2011) Molybdenum  
 1195 isotope fractionation in pelagic euxinia: evidence from the modern Black and Baltic  
 1196 Seas. *Chem. Geol.* **289**(1), 1–11.
- 1197 Neubert, N., Nägler, T. F., and Böttcher, M. E. (2008). Sulfidity controls molybdenum  
 1198 isotope fractionation into euxinic sediments: Evidence from the modern Black Sea.  
 1199 *Geology* **36**(10), 775–778.
- 1200 Nielsen, S. G., Rehkämper, M., Teagle, D. A., Butterfield, D. A., Alt, J. C., and Halliday,  
 1201 A. N. (2006). Hydrothermal fluid fluxes calculated from the isotopic mass balance of  
 1202 thallium in the ocean crust. *Earth Planet. Sci. Lett.* **251**(1), 120–133.
- 1203 Noffke, A., Hensen, C., Sommer, S., Scholz, F., Bohlen, L., Mosch, T., Graco, M., and  
 1204 Wallman, K. (2012) Benthic iron and phosphorus fluxes across the Peruvian oxygen  
 1205 minimum zone. *Limnol. Oceanogr.* **57**(3), 851–867.
- 1206 Oelkers, E. H., Jones, M. T., Pearce, C. R., Jeandel, C., Eiriksdottir, E. S., and Gislason, S.  
 1207 R. (2012). Riverine particulate material dissolution in seawater and its implications for  
 1208 the global cycles of the elements. *C. R. Geosci.* **344**(11), 646–651.

- 1209 Östlund, H.G. (1974). Expedition “Odysseus 65”: Radiocarbon age of Black Sea deep  
 1210 water. In *The Black Sea—Geology, chemistry, and biology* (eds. E.T. Degens and D.A.  
 1211 Ross). American Association of Petroleum Geologists Memoir **20**, 127–132.
- 1212 Özsoy, E., and Ünlüata, Ü. (1997). Oceanography of the Black Sea: a review of some  
 1213 recent results. *Earth-Sci. Rev.* **42**(4), 231–272.
- 1214 Peacock, C. L., and Moon, E. M. (2012). Oxidative scavenging of thallium by birnessite:  
 1215 explanation for thallium enrichment and stable isotope fractionation in marine  
 1216 ferromanganese precipitates. *Geochim. Cosmochim. Acta* **84**, 297–313.
- 1217 Pearce, C. R., Jones, M. T., Oelkers, E. H., Pradoux, C., and Jeandel, C. (2013). The effect  
 1218 of particulate dissolution on the neodymium (Nd) isotope and Rare Earth Element  
 1219 (REE) composition of seawater. *Earth Planet. Sci. Lett.* **369**, 138–147.
- 1220 Peterson, L. C, Haug, G. H., Murray, R. W., Yarincik, K. M., King, J. W., Bralower, T. J.,  
 1221 Kameo, K., Rutherford, S. D., and Pearce, R. B. (2000) Late Quaternary stratigraphy  
 1222 and sedimentation at Site 1002, Cariaco Basin (Venezuela). *Proc. ODP - Scientific*  
 1223 *Results* **165**, 85–99.
- 1224 Poulson-Brucker R., McManus J., Severmann S. and Berelson W. (2009) Molybdenum  
 1225 behavior during early diagenesis: insights from Mo isotopes. *Geochem. Geophys.*  
 1226 *Geosyst.* **10**(6), Q06010.
- 1227 Prospero, J. M. (1996). Saharan dust transport over the North Atlantic Ocean and  
 1228 Mediterranean: an overview. In *The impact of desert dust across the Mediterranean*  
 1229 (eds. S. Guerzoni and R. Chester). Springer, Netherlands. pp. 133–151.
- 1230 Reinhard, C. T., Planavsky, N. J., Wang, X., Fischer, W. W., Johnson, T. M., and Lyons,  
 1231 T. W. (2014) The isotopic composition of authigenic chromium in anoxic marine  
 1232 sediments: A case study from the Cariaco Basin. *Earth Planet. Sci. Lett.* **407**, 9–18.
- 1233 Resing, J. A., Sedwick, P. N., German, C. R., Jenkins, W. J., Moffett, J. W., Sohst, B. M.,  
 1234 and Tagliabue, A. (2015). Basin-scale transport of hydrothermal dissolved metals  
 1235 across the South Pacific Ocean. *Nature* **523**(7559), 200–203.
- 1236 Roshan, S., and Wu, J. (2015). The distribution of dissolved copper in the tropical-  
 1237 subtropical north Atlantic across the GEOTRACES GA03 transect. *Mar. Chem.* **176**,  
 1238 189–198.
- 1239 Roshan, S., Wu, J., and Jenkins, W. J. (2016). Long-range transport of hydrothermal  
 1240 dissolved Zn in the tropical South Pacific. *Mar. Chem.* **183**, 25–32.
- 1241 Rudnick R. and Gao S. (2003) Composition of the continental crust. *Treatise Geochem.* **3**,  
 1242 1–64.
- 1243 Ryan, B. M., Kirby, J. K., Degryse, F., Scheiderich, K., and McLaughlin, M. J. (2014).  
 1244 Copper isotope fractionation during equilibration with natural and synthetic ligands.  
 1245 *Environ. Sci. Technol.* **48**(15), 8620–8626.
- 1246 Saager, P. M., De Baar, H. J., & Howland, R. J. (1992). Cd, Zn, Ni and Cu in the Indian  
 1247 Ocean. *Deep Sea Res.* **39**(1), 9-35.
- 1248 Saager, P. M., Schijf, J., and de Baar, H. J. (1993). Trace-metal distributions in seawater  
 1249 and anoxic brines in the eastern Mediterranean Sea. *Geochim. Cosmochim. Acta* **57**(7),  
 1250 1419–1432.
- 1251 Sander, S. G., and Koschinsky, A. (2011). Metal flux from hydrothermal vents increased  
 1252 by organic complexation. *Nat. Geosci.* **4**(3), 145–150.

- 1253 Sansone, F. J., Graham, A. W., and Berelson, W. M. (2004). Methane along the western  
1254 Mexican margin. *Limnol. Oceanogr.* **49**(6), 2242–2255.
- 1255 Sarbas, B., and Nohl, U. (2009) The GEOROC database – a decade of “online  
1256 Geochemistry”. *Geochim. Cosmochim. Acta* **73**(13) Supplement, A1158.
- 1257 Sawlan, J. J., and Murray, J. W. (1983). Trace metal remobilization in the interstitial  
1258 waters of red clay and hemipelagic marine sediments. *Earth Planet. Sci. Lett.* **64**(2),  
1259 213–230.
- 1260 Schlitzer., R. (2015) Ocean Data View, odv.awi.de
- 1261 Schmitt, A. D., Chabaux, F., and Stille, P. (2003). The calcium riverine and hydrothermal  
1262 isotopic fluxes and the oceanic calcium mass balance. *Earth Planet. Sci. Lett.* **213**(3),  
1263 503–518.
- 1264 Scholz, F., Hensen, C., Noffke, A., Rohde, A., Liebetrau, V., and Wallmann, K. (2011)  
1265 Early diagenesis of redox-sensitive trace metals in the Peru upwelling area – response  
1266 to ENSO-related oxygen fluctuations in the water column. *Geochim. Cosmochim. Acta*  
1267 **75**(22), 7257–7276.
- 1268 Scholz, F., McManus, J., and Sommer, S. (2013) The manganese and iron shuttle in a  
1269 modern euxinic basin and implications for molybdenum cycling at euxinic ocean  
1270 margins. *Chem. Geol.* **355**, 56–68.
- 1271 Scholz, F., Severmann, S., McManus, J., and Hensen, C. (2014) Beyond the Black Sea  
1272 paradigm: The sedimentary fingerprint of an open-marine iron shuttle. *Geochim.*  
1273 *Cosmochim. Acta* **127**, 368–380.
- 1274 Schunck, H., Lavik, G., Desai, D. K., Grøkopf, T., Kalvelage, T., Löscher, C. R., Paulmier,  
1275 A., Contreras, S., Siegel, H., Holtappels, M., Rosenstiel, P., Schilhabel, M. B., Graco,  
1276 M., Schmitz, R. A., Kuypers, M. M. M., and LaRoche, J. (2013) Giant Hydrogen  
1277 Sulfide Plume in the Oxygen Minimum Zone off Peru Supports  
1278 Chemolithoautotrophy. *PLoS ONE* **8**(8), e68661.
- 1279 Schwalbach, J. R., and Gorsline, D. S. (1985). Holocene sediment budgets for the basins of  
1280 the California continental borderland. *J. Sed. Res.* **55**(6).
- 1281 Severmann, S., Lyons, T. W., Anbar, A., McManus, J., and Gordon, G. (2008) Modern  
1282 iron isotope perspective on the benthic iron shuttle and the redox evolution of ancient  
1283 oceans. *Geology* **36**(6), 487–490.
- 1284 Severmann, S., McManus, J., Berelson, W. M., and Hammond, D. E. (2010). The  
1285 continental shelf benthic iron flux and its isotope composition. *Geochim. Cosmochim.*  
1286 *Acta* **74**(14), 3984–4004.
- 1287 Shank, G. C., Skrabal, S. A., Whitehead, R. F., and Kieber, R. J. (2004a). Strong copper  
1288 complexation in an organic-rich estuary: the importance of allochthonous dissolved  
1289 organic matter. *Mar. Chem.* **88**(1), 21–39.
- 1290 Shank, G. C., Skrabal, S. A., Whitehead, R. F., Avery, G. B., and Kieber, R. J. (2004b).  
1291 River discharge of strong Cu-complexing ligands to South Atlantic Bight waters. *Mar.*  
1292 *Chem.* **88**(1), 41–51.
- 1293 Shaw, T. J., Gieskes, J. M., and Jahnke, R. A. (1990) Early diagenesis in differing  
1294 depositional environments: The response of transition metals in pore water. *Geochim.*  
1295 *Cosmochim. Acta* **54**(5), 1233–1246.

- 1296 Sherman, D. M. (2013). Equilibrium isotopic fractionation of copper during  
 1297 oxidation/reduction, aqueous complexation and ore-forming processes: Predictions  
 1298 from hybrid density functional theory. *Geochim. Cosmochim. Acta* **118**, 85–97.
- 1299 Sholkovitz, E. R., P. N. Sedwick, and T. M. Church (2010). On the fractional solubility of  
 1300 copper in marine aerosols: Toxicity of aeolian copper revisited, *Geophys. Res. Lett.*  
 1301 **37**, L20601, doi:10.1029/2010GL044817 .
- 1302 Silverberg, N., Martínez, A., Aguiñiga, S., Carriquiry, J. D., Romero, N., Shumilin, E., and  
 1303 Cota, S. (2004). Contrasts in sedimentation flux below the southern California Current  
 1304 in late 1996 and during the El Niño event of 1997–1998. *Estuar. Coast. Shelf Sci.*  
 1305 **59**(4), 575–587.
- 1306 Skrabal, S. A., Donat, J. R., and Burdige, D. J. (1997). Fluxes of copper-complexing  
 1307 ligands from estuarine sediments. *Limnol. Oceanogr.* **42**(5), 992–996.
- 1308 Skrabal, S. A., Donat, J. R., and Burdige, D. J. (2000). Pore water distributions of  
 1309 dissolved copper and copper-complexing ligands in estuarine and coastal marine  
 1310 sediments. *Geochim. Cosmochim. Acta* **64**(11), 1843–1857.
- 1311 Smith, R. W., Bianchi, T. S., Allison, M., Savage, C., and Galy, V. (2015). High rates of  
 1312 organic carbon burial in fjord sediments globally. *Nat. Geosci.* **8**(6), 450–453.
- 1313 Stott, L. D., Berelson, W., Douglas, R., and Gorsline, D. (2000). Increased dissolved  
 1314 oxygen in Pacific intermediate waters due to lower rates of carbon oxidation in  
 1315 sediments. *Nature* **407**(6802), 367–370.
- 1316 Stramma, L., Johnson, G. C., Sprintall, J., and Mohrholz, V. (2008). Expanding oxygen-  
 1317 minimum zones in the tropical oceans. *Science* **320**(5876), 655–658.
- 1318 Takano, S., Tanimizu, M., Hirata, T., and Sohrin, Y. (2014). Isotopic constraints on  
 1319 biogeochemical cycling of copper in the ocean. *Nat. commun.* **5**, 5663.
- 1320 Tankéré S. P. C., Muller F. L. L., Burton J. D., Statham P. J., Guieu C. and Martin J. M.  
 1321 (2001) Trace metal distributions in shelf waters of the northwestern black sea. *Cont.*  
 1322 *Shelf Res.* **21**(13–14), 1501–1532.
- 1323 Taylor S. and McLennan S. (1985). The continental crust: its composition and evolution.
- 1324 Thompson, C. M., and Ellwood, M. J. (2014). Dissolved copper isotope biogeochemistry  
 1325 in the Tasman Sea, SW Pacific Ocean. *Mar. Chem.* **165**, 1–9.
- 1326 Thunell, R. C., Tappa, E., and Anderson, D. M. (1995). Sediment fluxes and varve  
 1327 formation in Santa Barbara Basin, offshore California. *Geology* **23**(12), 1083–1086.
- 1328 Thunell, R. C., Varela, R., Llano, M., Collister, J., Karger, F. M., and Bohrer, R. (2000).  
 1329 Organic carbon fluxes, degradation, and accumulation in an anoxic basin: sediment  
 1330 trap results from the Cariaco Basin. *Limnol. Oceanogr.* **45**(2), 300–308.
- 1331 Tipper E., Gaillardet J., Galy A., Louvat P., Bickle M. and Capmas F. (2010) Calcium  
 1332 isotope ratios in the world’s largest rivers: a constraint on the maximum imbalance of  
 1333 oceanic calcium fluxes. *Global Biogeochem. Cycles* **24**(3).
- 1334 Tipper E., Galy A., Gaillardet J., Bickle M., Elderfield H. and Carder E. (2006) The  
 1335 magnesium isotope budget of the modern ocean: constraints from riverine magnesium  
 1336 isotope ratios. *Earth Planet. Sci. Lett.* **250**(1), 241–253.
- 1337 Tribovillard, N., Hatem, E., Averbuch, O., Barbecot, F., Bout-Roumazielles, V., and  
 1338 Trentesaux, A. (2015). Iron availability as a dominant control on the primary

- 1339 composition and diagenetic overprint of organic-matter-rich rocks. *Chem. Geol.* **401**,  
1340 67–82.
- 1341 Trocine R. P. and Trefry J. H. (1988) Distribution and chemistry of suspended particles  
1342 from an active hydrothermal vent site on the Mid-Atlantic Ridge at 26 N. *Earth*  
1343 *Planet. Sci. Lett.* **88**(1–2), 1–15.
- 1344 Vance D., Archer C., Bermin J., Perkins J., Statham P. J., Lohan M. C., Ellwood M. J. and  
1345 Mills R. A. (2008) The copper isotope geochemistry of rivers and the oceans. *Earth*  
1346 *Planet. Sci. Lett.* **274**(1–2), 204–213.
- 1347 Vance, D., Little, S. H., Archer, C., Cameron, V., Andersen, M. B., Rijkenberg, M. J., and  
1348 Lyons, T. W. (2016a). The oceanic budgets of nickel and zinc isotopes: the importance  
1349 of sulfidic environments as illustrated by the Black Sea. *Phil. Trans. R. Soc. A*,  
1350 **374**(2081), 20150294.
- 1351 Vance, D., Matthews, A., Keech, A., Archer, C., Hudson, G., Pett-Ridge, J., and  
1352 Chadwick, O. A. (2016b). The behaviour of Cu and Zn isotopes during soil  
1353 development: Controls on the dissolved load of rivers. *Chem. Geol.* **445**, 36–53.
- 1354 van Geen, A., Zheng, Y., Bernhard, J. M., Cannariato, K. G., Carriquiry, J., Dean, W. E., ...  
1355 and Pike, J. (2003). On the preservation of laminated sediments along the western  
1356 margin of North America. *Paleoceanography* **18**(4).
- 1357 Wasylenki, L. E., Weeks, C. L., Bargar, J. R., Spiro, T. G., Hein, J. R., and Anbar, A. D.  
1358 (2011). The molecular mechanism of Mo isotope fractionation during adsorption to  
1359 birnessite. *Geochim. Cosmochim. Acta* **75**(17), 5019–5031.
- 1360 Welch, S. A., Beard, B. L., Johnson, C. M., and Braterman, P. S. (2003). Kinetic and  
1361 equilibrium Fe isotope fractionation between aqueous Fe (II) and Fe (III). *Geochim.*  
1362 *Cosmochim. Acta* **67**(22), 4231–4250.
- 1363 Wells, M. L., Kozelka, P. B., and Bruland, K. W. (1998). The complexation of dissolved  
1364 Cu, Zn, Cd and Pb by soluble and colloidal organic matter in Narragansett Bay, RI.  
1365 *Mar. Chem.* **62**(3), 203–217.
- 1366 Werne, J. P., Lyons, T. W., Hollander, D. J., Formolo, M. J., and Sinninghe Damsté, J. S.  
1367 (2003) Reduced sulfur in euxinic sediments of the Cariaco Basin: sulfur isotope  
1368 constraints on organic sulfur formation. *Chem. Geol.* **195**(1–4), 159–179.
- 1369 Windom, H., Wallace, G., Smith, R., Dudek, N., Maeda, M., Dulmage, R., and Storti, F.  
1370 (1983). Behavior of copper in southeastern United States estuaries. *Mar. Chem.* **12**(2-  
1371 3), 183–193.
- 1372 Xue, Z., Rehkämper, M., Horner, T. J., Abouchami, W., Middag, R., van de Flierdt, T., and  
1373 de Baar, H. J. (2013). Cadmium isotope variations in the Southern Ocean. *Earth*  
1374 *Planet. Sci. Lett.* **382**, 161–172.
- 1375 Yarincik, K. M., Murray, R. W., and Peterson, L. C. (2000). Climatically sensitive eolian  
1376 and hemipelagic deposition in the Cariaco Basin, Venezuela, over the past 578,000  
1377 years: Results from Al/Ti and K/Al. *Paleoceanography* **15**(2), 210–228.
- 1378 Zheng, Y., Anderson, R. F., van Geen, A., and Kuwabara, J. (2000). Authigenic  
1379 molybdenum formation in marine sediments: a link to pore water sulfide in the Santa  
1380 Barbara Basin. *Geochim. Cosmochim. Acta* **64**(24), 4165–4178.
- 1381 Zhu, P., and Macdougall, J. D. (1998). Calcium isotopes in the marine environment and the  
1382 oceanic calcium cycle. *Geochim. Cosmochim. Acta* **62**(10), 1691–1698.

1383 Zhu, X. K., Guo, Y., Williams, R. J. P., O'nioms, R. K., Matthews, A., Belshaw, N. S., ...  
1384 and Salvato, B. (2002). Mass fractionation processes of transition metal isotopes.  
1385 *Earth Planet. Sci. Lett.* **200**(1), 47–62.